Electrospray Ionization

12

Learning Objectives

- Electrospray – a method of ion formation at atmospheric pressure
- Interfacing atmospheric pressure ionization to analyzer high vacuum
- Spraying of electrolytic solutions by action of an electrostatic field
- Processes of ion liberation from electrolytic solutions
- Formation of multiply charged ions and charge deconvolution
- Small molecules analysis by electrospray ionization
- High-mass and high-polarity capabilities of electrospray ionization

Electrospray ionization (ESI) is the most prominent technique among the group of *atmospheric pressure ionization* (API) methods, some of which have already been discussed in the context of chemical ionization at atmospheric pressure (APCI, Sects. 7.8 and 7.9). ESI is the method of choice for *liquid chromatography-mass spectrometry coupling* (LC-MS, Chap. 14) [1–4]. In fact, ESI and *matrix-assisted laser desorption/ionization* (MALDI, Chap. 11) have provided the means for expanding the application of MS into the fields of biology and the biomedical sciences, and currently, they are the most frequently employed ionization methods in MS [1, 2, 4–11].

ESI "is a soft ionization technique that accomplishes the transfer of ions from solution to the gas phase. The technique is extremely useful for the analysis of large, non-volatile, chargeable molecules such as proteins and nucleic acid polymers" [10–15]. In contrast to *fast atom bombardment* (FAB, Chap. 10), in ESI the solution is composed of a volatile solvent containing the ionic analyte at very low concentration, typically 10^{-6}–10^{-4} M. In addition, the transfer of ions from the condensed phase into the state of isolated gas-phase ions starts at atmospheric pressure and

J.H. Gross, *Mass Spectrometry*, DOI 10.1007/978-3-319-54398-7_12

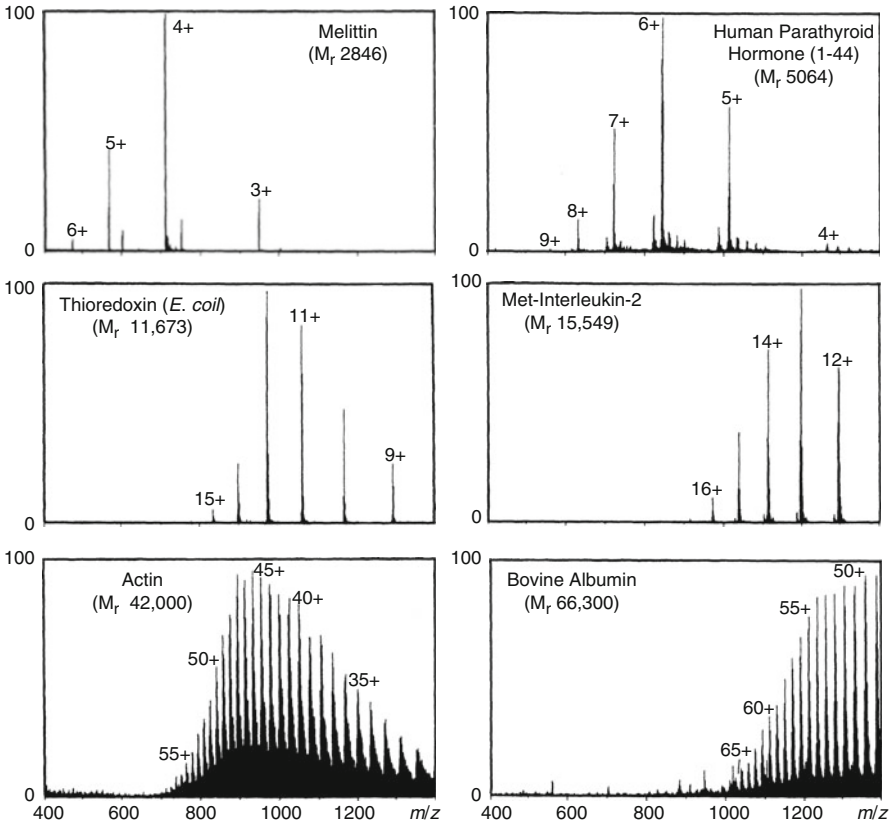

Fig. 12.1 Relationship between the mass of peptides and proteins and the number of ionic charges under ESI conditions (Adapted from Ref. [18] by permission. © American Chemical Society, 1990)

incrementally proceeds into the high vacuum of the mass analyzer [6, 16–18]. This results in a marked softness of ionization and makes ESI the "wings for molecular elephants" [19]. Another reason for the extraordinary high-mass capability of ESI [15, 20, 21] is founded in the characteristic formation of multiply charged ions in case of high-mass analytes [15, 18, 22]. Multiple charging also folds up the m/z scale by the number of charges, and thus, shifts the ions into an m/z range accessible by most mass analyzers (Fig. 12.1 and Sect. 3.8)

ESI serves equally well for small polar molecules, ionic metal complexes [23–25], and other soluble inorganic analytes [26]. So let's start exploring the ESI route with this promising outlook in mind.

Beyond the usual *m*/*z*: Most high-mass analytes examined by ESI readily form multiply charged ions. Normally, it is therefore sufficient in ESI-MS to cover the range up to *m*/*z* 3000 for the detection of ions. This does not preclude, however, that ESI can produce ions of much higher *m*/*z* [27, 28]; even ions at *m*/*z* 85,000 have been observed [29].

12.1 Route Leading to Electrospray Ionization

ESI in its current state-of-the-art has not resulted from a straightforward development. It has many predecessors, some of which having been successful at their time, while others were rather short-lived methods replaced as soon as more sensitive or more robust techniques appeared [30]. Nonetheless, the development of all those techniques aimed at both the direct coupling of liquid chromatography to mass spectrometry and the access to highly polar or even ionic analytes.

Following this historical sketch of milestones along the way to ESI, the below sections will emphasize the construction of ESI interfaces, the process of electrospray as such, and the pathways of ion liberation from the liquid phase into the state of isolated gas phase ions.

12.1.1 Atmospheric Pressure Ionization and Related Methods

The first technique, *atmospheric pressure ionization* (API), was presented as early as 1973 by the Horning group [31]. Just 1 year later, the same group introduced a largely improved variant as *atmospheric pressure chemical ionization* (APCI) [32]. In 2000, *atmospheric pressure photoionization* (APPI) was developed to expand the range of applications to analytes of lower polarity [33]. As API, APCI, and APPI essentially rely on chemical ionization processes, these were already discussed in Sects. 7.8 and 7.9. Both techniques, APCI and APPI, are frequently employed. Nowadays, *atmospheric pressure ionization* has been transformed into a collective term for all techniques where ion generation occurs at atmospheric pressure.

12.1.2 Thermospray

In *Thermospray* (TSP) [34–36] a solution of the analyte and a volatile buffer, usually 0.1 M ammonium acetate, is evaporated from a heated capillary at a liquid flow of 1–2 ml min^{-1} into a heated chamber (>600 °C), hence the term. As the solvent evaporates, the analyte starts to form adducts with ions from the buffer salt. While most of the neutrals are removed by a vacuum pump, the ions are extracted orthogonally from their main axis of motion by use of an electrostatic potential. The

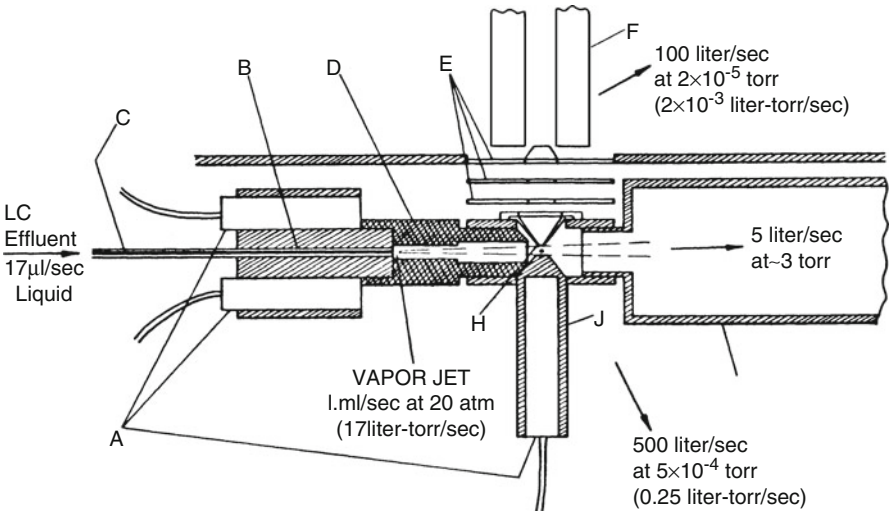

Fig. 12.2 Thermospray interface. *A* cartridge heater; *B* copper block brazed to stainless steel capillary; *C* capillary; *D* copper tube; *E* ion lenses; *F* quadrupole mass analyzer; *G* line to rotary vane pump; *H* ion exit aperture; *J* source heater (Reproduced from Ref. [35] by permission. © American Chemical Society, 1983)

ions are transferred into a quadrupole mass analyzer through a pinhole of about 25 µm in diameter (Fig. 12.2). A quadrupole is employed due to its tolerance to poor vacuum conditions.

As the pure TSP mode only works with high-polarity solvents in the presence of a buffer salt, modified modes of operation were developed to expand the use of TSP ion sources to lower-polarity systems. One approach used an electrical discharge in the vapor phase [37], while another operated an electron-emitting filament in the expanding gas cloud. Either addition essentially emulated APCI on the TSP interface. With this added versatility, TSP meant a breakthrough for LC-MS [38]. Nonetheless, with the advent of ESI, TSP interfaces vanished rather quickly from the laboratories.

Only halfway API: Strictly speaking, thermospray is not really an API method because the analyte solution is sprayed into a rough vacuum of several hundred Pa instead of spraying at full atmospheric pressure.

12.1.3 Electrohydrodynamic Ionization

An electrolytic solution of sufficiently low volatility can be transferred into the vacuum without sudden evaporation and then be sprayed from a fine capillary by the action of a strong electrostatic field. This is known as *electrohydrodynamic ionization* (EHI) [39, 40]. EHI results from the interaction of the field with the

liquid meniscus at the end of the capillary tube [41, 42]. A mist of micrometer-sized electrically charged droplets expands into the vacuum at supersonic speed. The droplets shrink upon evaporation of solvent. Shrinking causes the charge density on their surface to exceed the *Rayleigh limit* of stability [43], i.e., the surface tension is overcome by electrostatic repulsion. The electric forces then tear the droplets apart. The sequence of droplet shrinking and subsequent disintegration into smaller subunits occurs repeatedly and eventually leads to the formation of isolated gas-phase ions.

Even though EHI ion sources are at hand by simply replacing the field emitter of a field desorption (FD) source with a capillary tube (Sect. 8.3) [44, 45], EHI never managed to become established in organic mass spectrometry. This is most probably due to its limitation to low-volatile solvents. Nonetheless, EHI has been applied to analyze polymers [46] and is still used to generate primary ions in massive cluster impact (MCI) mass spectrometry (Sect. 10.8).

EHI has important features in common with ESI:

- An electrolytic solution is sprayed by the mere action of an electrostatic field.
- Spraying forms a mist of electrically highly charged droplets.
- Analyte ions are liberated from solution phase into the gas phase.
- Analyte ions thus have already to exist before spraying of the solution.

12.1.4 Electrospray Ionization

The conceptual development of electrospray ionization by the Dole group [47] actually preceded API, TSP, and EHI by several years [48]. The underlying principle of ESI, which it shares with EHI, even dates back to work by Zeleny in 1917 [41] and Taylor in 1964 [42].

In ESI, similar to EHI, a mist of micrometer-sized electrically charged droplets is generated. The repetitive shrinking and droplet disintegration are also observed under ESI conditions. In contrast to EHI, the process of electrostatic spraying is sustained at atmospheric pressure. The electrostatically charged aerosol is then continuously passed into the mass analyzer by means of a differentially pumped interface. The limitation of Dole's experiments was that the ions of the electrosprayed high-molecular-weight polystyrene used by his group could not be detected with his mass spectrometers [47–49]. It took years of work for the Fenn group and lasted until the late 1980s to fully realize that analytes of 100–2000 u molecular weight can be readily analyzed with a quadrupole attached to a properly constructed ESI interface [16, 19, 50]. To avoid freezing of the aerosol droplets under the conditions of adiabatic expansion on their transition from the atmosphere into the vacuum, sufficient energy supply turned out to be crucial. The heat may either be delivered by a heated countercurrent gas stream or by a heated capillary being part of the interface. Until today, all ESI sources make use of the one or the other way of heating the aerosol. The fact that ESI can be run with almost any standard solvent is another key to its tremendous success [19].

Open to the atmosphere: Any atmospheric pressure ionization method, i.e., ESI as well as APCI and APPI, requires an uninterrupted transport of ions from ambient pressure into the high vacuum of a mass analyzer. An API interface has thus to accomplish the efficient transfer of ions while at the same time it has to remove the concomitant gas flow to preserve the analyzer vacuum. This is accomplished by means of differential pumping.

12.2 Interfaces for Electrospray Ionization

12.2.1 Basic Design Considerations

The first electrospray-mass spectrometry interface was designed by the Fenn group in the mid 1980s [16, 50–52]. In this interface, the dilute sample solution is supplied by a syringe pump through a hypodermic needle – the *spray capillary* – at a flow of 5–20 µl min^{-1}. The spray capillary is kept at a potential of 3–4 kV relative to a surrounding cylindrical electrode (Fig. 12.3). Then, the electrosprayed aerosol expands into a countercurrent stream of hot nitrogen gas serving as a heat supply for vaporization of the solvent. A small portion of the sprayed material enters the aperture of a short capillary (0.2 mm inner diameter, 60 mm length) interfacing the atmospheric pressure spray zone to the first pumping stage ($\approx 10^2$ Pa) that is entered by the gas in a free jet expansion. Most of the gas expanding from the desolvating aerosol is pumped off by a rotary vane pump as it exits from the capillary. A minor portion passes through the orifice of a skimmer (a cone-shaped electrode with a small aperture at its apex) into the high vacuum behind ($\approx 10^{-3}$–10^{-4} Pa). At this stage, desolvation of the ions is completed, while the ions are focused into a mass analyzer. Suitable potentials applied to capillary, skimmer, and lenses behind

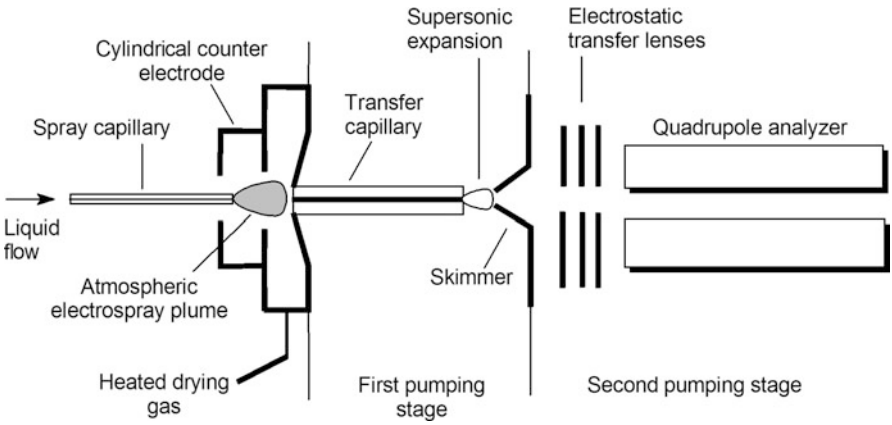

Fig. 12.3 Schematic of an early electrospray interface design [16]

provide an effective transfer of ions through the interface, while the neutral gas is not affected and exits via the vacuum system.

Modern *ESI interfaces* are designed in many variations of this basic scheme [53, 54]. They may either use a *heated transfer capillary* or a *countercurrent stream of hot nitrogen* (sometimes called *curtain gas*) to enforce solvent evaporation [55]. These differences can affect a system's robustness and the degree of cluster ion formation with a particular ESI interface [56, 57]. Whatever the details, they are all derived from a *nozzle-skimmer system* initially proposed by Kantrowitz and Grey [58] that delivers an intense cool molecular jet into the high vacuum environment [47, 50, 59].

The adiabatic expansion of the gas upon entering the first pumping stage reduces random motion of the particles due to extensive cooling. Furthermore, a portion of the thermal motion is converted into directed flow by the nozzle-skimmer arrangement. In summary, this causes the heavier analyte ion-containing solvent clusters to travel close to the center of the flight path through the interface, while light solvent molecules escape from the jet [48]. Thus, the skimmer orifice is not just statistically passed by all sorts of particles but rather selectively by ionic constituents of the adiabatically expanding plume.

A comparison of API interface concepts – all of them in use today – is provided in Fig. 12.4 [60]. A closer discussion of the particular approaches will follow later in this chapter.

Ions already have to be there: ESI requires analyte ions to be present in the sample solution because ESI does not actively create ions. In fact, ESI is rather a method of ion transfer than a true ionization method. Thus, ESI is in stark contrast to all other ionization methods currently in use (EI, CI, APCI, APPI, FAB, FD, MALDI, DART). Therefore, *electrospray ionization* (ESI) is also simply referred to as *electrospray* (ES) and *ESI ion sources* may better be termed *ESI interfaces*.

12.2.2 Adaptation of ESI to Different Flow

The actual process of "electrospraying" disperses a liquid into an aerosol, which works best at flows of 1–20 µl min^{-1}. This sets certain limits to its use as an LC-MS interface in respect to solvent properties such as volatility and polarity. Consequently, a number of sprayer design modifications have led to an expansion of the range of ESI applications (Fig. 12.5).

The design of a *pneumatically assisted* ESI interface differs from the simple electrospray interface in that it provides a pneumatic assistance for the spray process. This is achieved by supplying a concentric flow of an inert gas such as nitrogen around the electrospray plume [61–63]. Assistance by a *nebulizer gas* stream of about 1–5 l min^{-1} allows for higher liquid flow and for a reduced influence of the surface tension of the solvent [64]. Pneumatically assisted ESI can

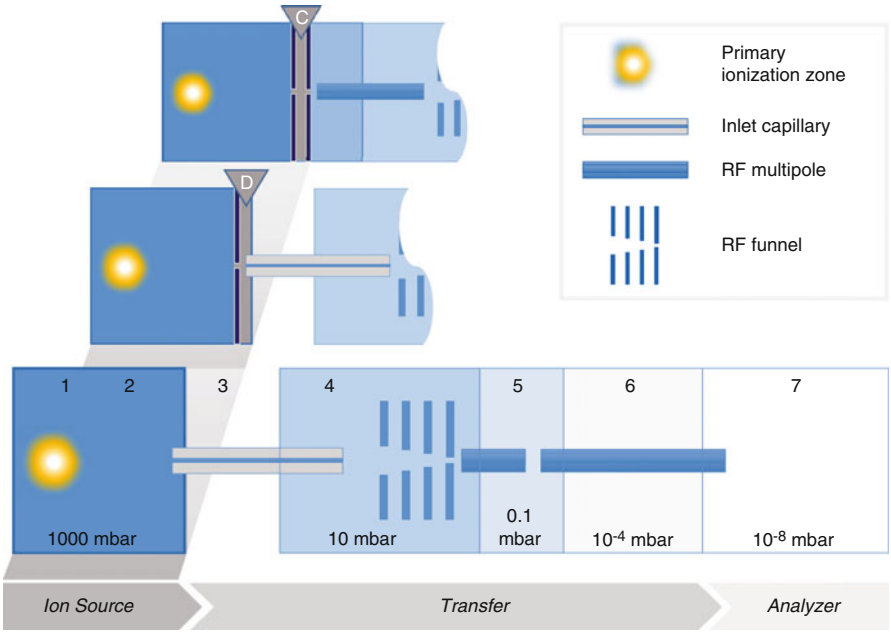

Fig. 12.4 Comparison of basic API interface designs and their functional regions: (*1*) Ion formation, (*2*) thermalization, (*3*) turbulent entry flow, (*4*) expansion into vacuum, (*5–6*) ion guides and eventually activation by CID, (*7*) mass analyzer. Indicated pressures may vary considerably. RF funnels and RF multipoles are not to scale and various voltages are normally applied to these ion optical elements. *Bottom:* ion source coupled via a capillary to the vacuum system of the analyzer, e.g., Thermo-Fisher. *Center*: same as previous but additional directed "dry" (*D*) gas flow through a biased sampling electrode, termed *spray shield* in instruments by Bruker Daltonics or Agilent Technologies. *Top*: ion source coupled via orifices to the vacuum system of the analyzer; additionally a curtain (*C*) gas flow is directed into the source, and a differential pumping stage (AB SCIEX) (Reproduced from Ref. [60] with permission. © Springer, 2014)

accommodate flows of 10–200 μl min^{-1}. In fact, all modern ESI interfaces are equipped with a nebulizer gas or *sheath gas* line enclosing the spray capillary. Thus, most routine ESI measurements are actually performed using pneumatically assisted ESI. In pneumatically assisted ESI the purpose of the high voltage is almost reduced to the mere supply of electric charging of the droplets. For highly polar solutions at very low liquid flow, nanoESI provides the better technique (next section).

For *capillary zone electrophoresis* (CZE) mass spectrometry coupling, another modification of an ESI sprayer has been developed. It uses a *sheath flow* or *make-up flow* of solvent for establishing the electrical contact at the CZE terminus, thus defining both the CZE and electrospray field gradients. The make-up flow also serves to adjust the low CZE flow to an ESI-compatible level.

This way, the composition of the electrosprayed liquid can be controlled independently of the CZE buffer, thereby enabling operation with buffers that could not

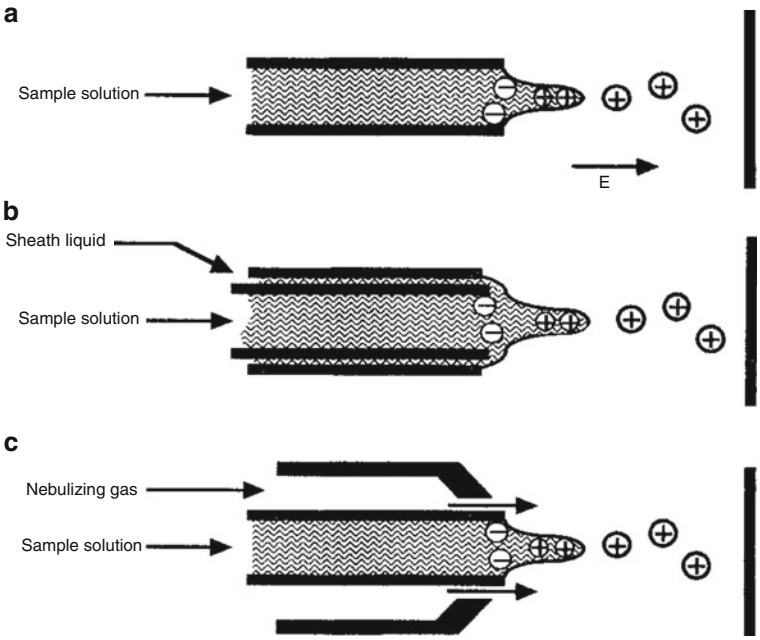

Fig. 12.5 Different sprayers for ESI. (**a**) Pure electrospray, (**b**) ESI with sheath liquid, (**c**) pneumatically-assisted ESI (Adapted from Ref. [6] (p. 109) by permission. © John Wiley & Sons, Inc., 1997)

be used previously, e.g., aqueous and high ionic strength buffers. In addition, the interface operation becomes independent of the CZE flow rate [65].

Ion spray? *Pneumatically assisted electrospray* is also termed *ion spray* (ISP). However, the term ISP is not recommended in place of pneumatically-assisted ESI because ISP represents a mere modification of the ESI setup and is a company-specific term [66].

12.2.3 Improved Electrospray Configurations

Since the publication of the original design in the 1980s by the Fenn group, the ESI interface underwent various substantial improvements in

- robustness of operation during elongated periods of unattended operation,
- ion transmission from the sprayer into the mass analyzer,
- softness for effective ion desolvation without inducing fragmentation, and
- effectiveness of differential pumping.

Nonetheless, whatever the actual design, all of those interfaces still have some basic characteristics in common:

- electrostatic spraying of an electrolytic solution at atmospheric pressure,
- heat supply for solvent evaporation and ion desolvation,
- supersonic expansion into the first pumping stage, and
- differential pumping across three or sometimes four stages.

While early interfaces were intuitively aligned along the central axis from the spray capillary to the analyzer entrance, more recent designs employ spraying at an angle to the vacuum entrance. These arrangements have the advantage of largely reducing possible contamination, especially by preventing the clogging of capillaries and skimmers, which formerly was one of the most severe problems with the otherwise easy-to-use ESI interfaces. When analytes are accompanied by nonvolatile impurities, e.g., by buffer salts used to improve liquid chromatography or organic material as present in blood or urine samples, the deposition of this material can cause the rapid breakdown of the ESI interface.

These improved designs achieve a spatial separation of the deposition site of nonvolatized material and the location of the ion entrance into the mass spectrometer. Such designs include (*i*) spraying *off-axis*, (*ii*) guiding the desolvating microdroplets through *inflected paths*, and (*iii*) spraying at an angle up to *orthogonal* (Fig. 12.6) [66]. It is a great advantage of orthogonal spraying that the entrance of the interface may selectively collect small and highly charged droplets that present the best source of analyte ions. Larger and less-charged droplets are not sufficiently attracted by the extraction field at 90° angle and therefore miss the orifice.

The first commercial ESI interface using about 90° deflection is the Waters *z-spray*™ interface (Fig. 12.7). All modern electrospray interfaces employ a closely related configuration. The entrance region of Bruker and Agilent API interfaces, for example, comprises a grounded spray capillary, a counter electrode at high voltage, and a countercurrent flow of hot nitrogen around the orifice of the ion transfer capillary that is aligned close to right angle with respect to the sprayer (Fig. 12.8). Modern interfaces are also designed with easy cleaning in mind.

12.2.4 Advanced Atmospheric Pressure Interface Designs

We have already briefly encountered some of the modern atmospheric pressure interfaces as front-ends of mass analyzers in the context of instrumentation (Chap. 4) and tandem MS (Chap. 9). The actual configuration of such interfaces largely depends on the high vacuum requirements of the mass analyzer attached, e.g., simple two-stage differential pumping is sufficient for linear quadrupoles and quadrupole ion traps, while others demand for virtual absence of residual gas. Furthermore, company-specific technologies will govern certain parts of the ion transfer optics such as RF-only ion guides (Figs. 12.4 and 12.9).

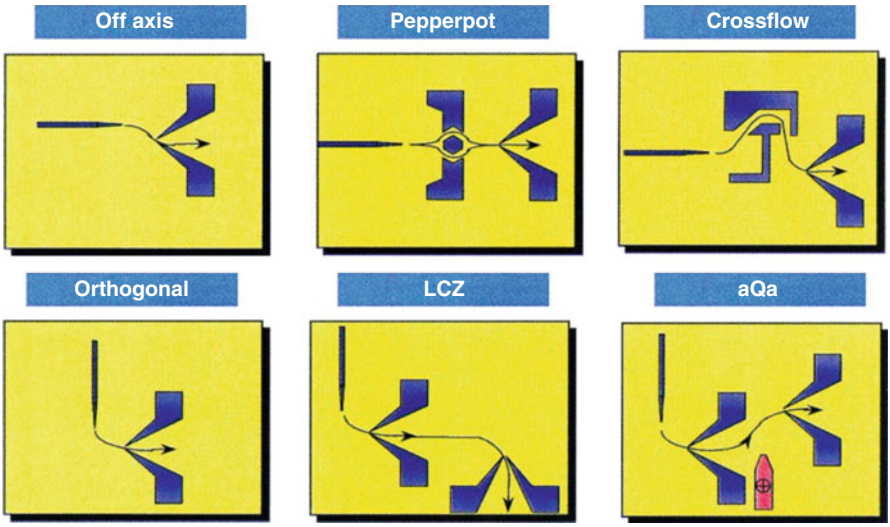

Fig. 12.6 Some strategies used in commercial API ion sources to increase solvent compatibility and system robustness. Some of these designs are (were) commercial brands: Pepperpot, Crossflow, and LCZ ("z-spray", Micromass); AQA (Thermo Finnigan) (Reproduced from Ref. [66] by permission. © John Wiley & Sons, 1999)

In recent years, so-called *ion funnels* are being used in place of the conventional skimmer cone electrode [67–69]. Ion funnels are radio frequency devices ($\leq$1 MHz) composed of a stack of dozens of ring electrodes, typically spaced about 3 mm apart along the ion funnel axis, with a central aperture of increasingly smaller diameter, e.g., from 20 mm at the opening to 1 mm at the exit. An RF voltage of equal amplitude but opposite phase (200–400 V) is supplied between adjacent electrodes. Similar to stacked ring ion guides (Sect. 4.10) this alignment of electrodes creates a field that pushes ions down a low electric field gradient far more effectively than the field gradient alone could do. As the apertures decrease along the device the ion packages are not only transported but – more importantly – are also radially confined. This is employed to focus ion beams through narrow apertures into the next differential pumping stage or into a mass analyzer [70, 71]. As ion funnels are best operated under the conditions of collisionally damped ion motion, i.e., at rough vacuum of 1–10 mbar (Sect. 4.4.4), they are perfectly compatible with the first pumping stage of ESI interfaces. Ion funnels increase the transmission of ESI interfaces, and accordingly, result in at least tenfold-improved overall sensitivity of the mass spectrometer as compared to sources with a skimmer electrode.

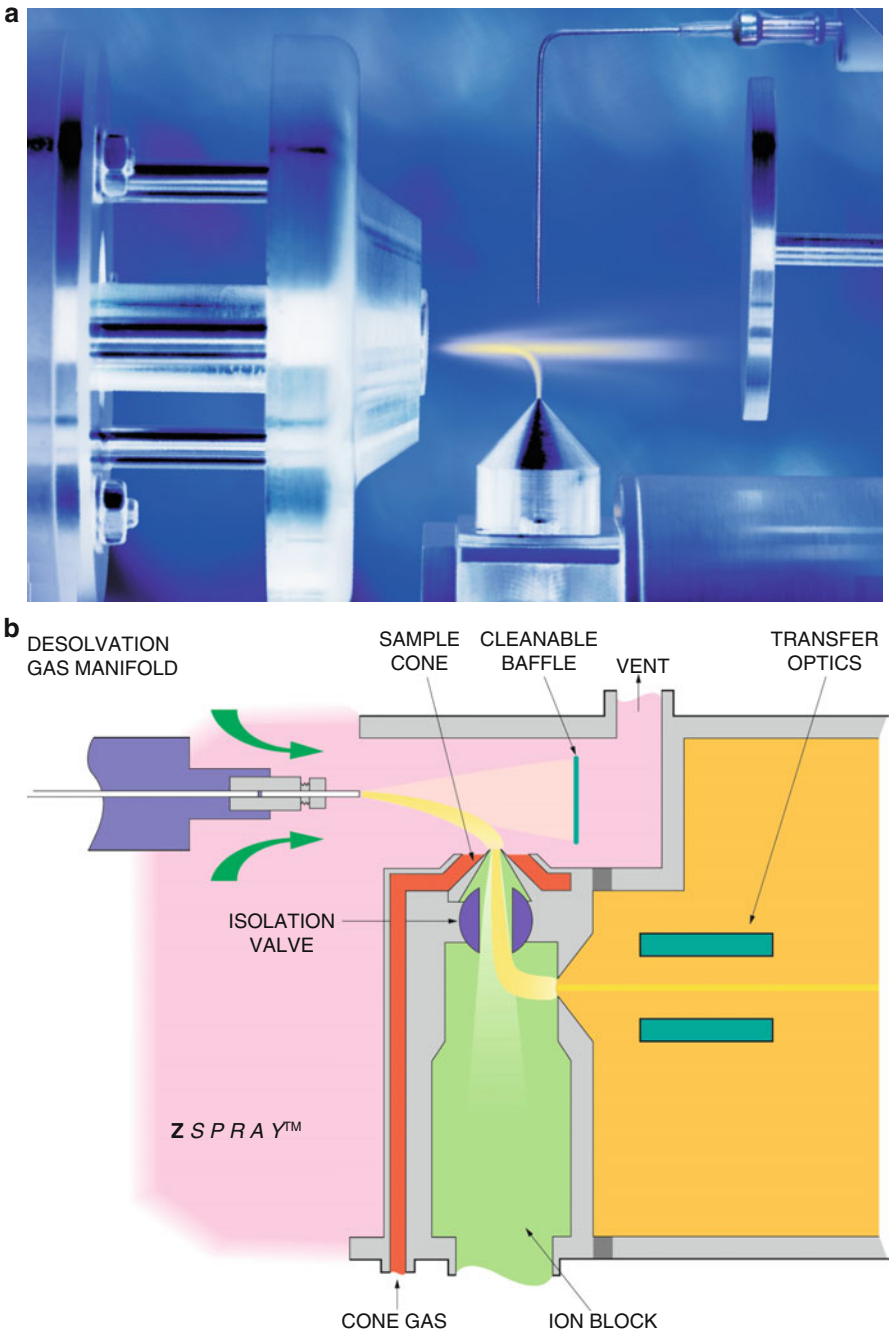

Fig. 12.7 Micromass *z*-spray interface. (**a**) Photograph of the actual spray from which charged constituents are extracted downwards into the entrance orifice. While large droplets and neutrals are traveling on a straight path toward the counter electrode, small highly charged droplets are attracted by the entrance at the cone-shaped electrode. (**b**) Schematic including the inner parts of the interface (By courtesy of Waters Corporation, MS Technologies, Manchester, UK)

Fig. 12.8 Atmospheric pressure side of the Bruker Apollo II API interface. (**a**) Spray shield in place, (**b**) removal of the spray shield shows an aerodynamically shaped cap on top of the transfer capillary, and (**c**) metal-coated section of the glass transfer capillary. The hot desolvation gas is supplied via six concentrically aligned ports around the transfer capillary. In operation, the sprayer would be aligned close to the spray shield as to direct the aerosol from top to bottom in an orientation close to right angle with respect to the transfer capillary. For the interior layout of this interface cf. Fig. 12.12

Multi-purpose API interfaces: There are no dedicated ESI interfaces anymore. All interfaces are constructed to be compatible with any variant of atmospheric pressure ionization by simply swapping the front part, e.g., an ESI sprayer for an APCI unit. The interface from the orifice at atmospheric pressure to the entry of the mass analyzer at high vacuum remains untouched. This enables quick method switching, avoids down time by interrupted vacuum, and ensures constant levels of mass resolving power and mass accuracy.

Two-stage off-axis ion funnels The next level of achieving efficient ion collection, transfer across pumping stages, and focusing is achieved by two-stage ion funnels in an off-axis alignment. Again, this exploits the fact that ions may easily be guided along potential gradients while neutrals are not affected. Thus, ions can be pushed out of the stream to follow a different track while neutrals are directed into an exhaust pipe, e.g., as in the Waters StepWave interface (Fig. 12.10).

12.2.5 Nozzle-Skimmer Dissociation

The rough vacuum of the first pumping stage, formerly the short zone between nozzle and skimmer, of an atmospheric pressure interface does not only provide

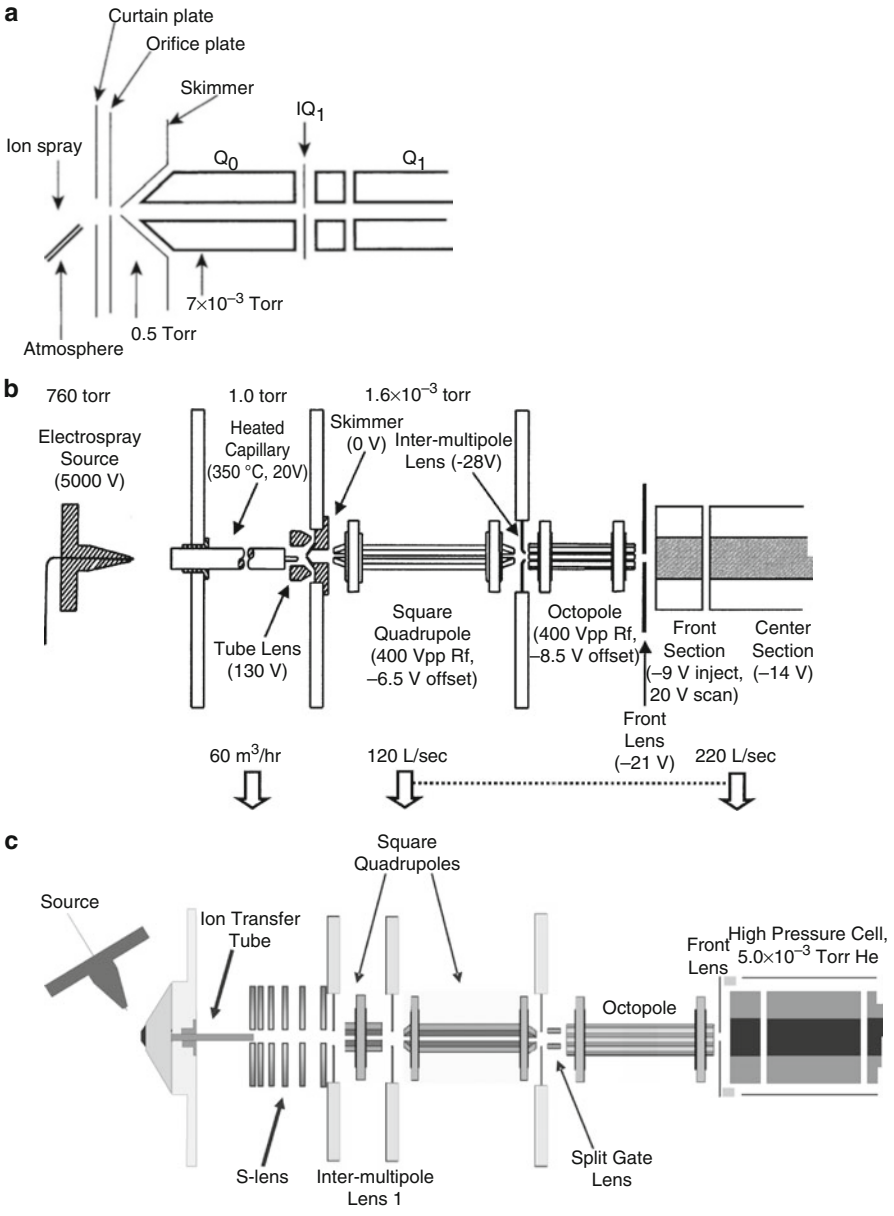

Fig. 12.9 Electrospray interfaces: (**a**) Setup for linear quadrupole and triple quadrupole instruments with 45° spray, heated countercurrent desolvation gas ("curtain gas"), orifice–skimmer setup for the first pumping stage, and RF-only quadrupole as ion guide in the second pumping stage. (**b**) On-axis spray on entrance of heated capillary serving as counter electrode, nozzle-skimmer arrangement, and RF-only multipole ion guides in front of an LIT. (**c**) Similar to (**b**) but the skimmer has been replaced by an ion-focusing lens system to improve transmission. This figure uses the front parts from Figs. 4.46, 4.50, and 9.28, respectively; reference to the according sources is given there

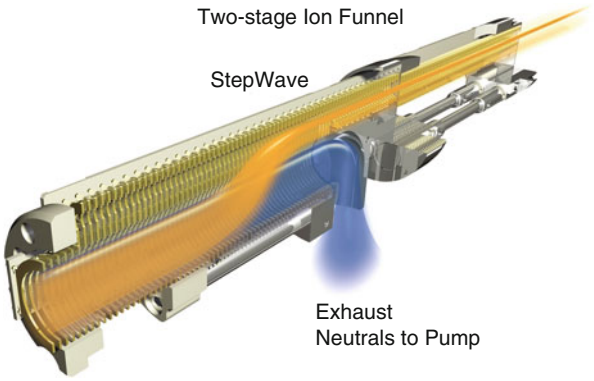

Fig. 12.10 Two-stage ion funnel with off-axis alignment for optimized transfer of ions (*orange cloud*) while neutral gas (*blue cloud*) is directed into an exhaust pipe. This particular setup is realized in the Waters StepWave interface (Adapted with permission of Waters MS Technologies, Manchester, 2016)

space for effective desolvation [72, 73], but can also be used to achieve fragmentation of the ions by *collision-induced dissociation* (CID, Sect. 9.3). While a comparatively high pressure in this region can effect collisional cooling (Sect. 4.4.4) rather than dissociative collisions [74], an increased voltage difference in this region enhances ion fragmentation by CID [72, 74, 75].

Nozzle-skimmer dissociation (NSD) or simply *skimmer CID* can

- strip off residual solvent molecules,
- achieve fragmentation of ions resulting in spectra similar to CI mode [76], and
- generate first-generation fragment ions for further tandem MS experiments.

The latter method provides a *pseudo* MS^3 operation on triple quadrupole or Q-TOF mass spectrometers [77–79]. Real MS^3 would require mass-selection prior to the first CID stage, too (for an example of pseudo MS^3 using NSD cf. Sect. 12.5.1). A programmable CID routine delivers ESI mass spectra with a variable degree of fragmentation from a single run [75, 77, 78, 80].

Unwanted CID Even a moderate voltage drop between nozzle and skimmer can cause the elimination of weakly bonded substituents such as CO_2 in case of carbon dioxide-protected deprotonated *N*-heterocycles. In particular, $SnMe_3$-substituted anions such as 2-(trismethylstannyl)pyrrole-*N*-carbamate exhibit strong variations in the $[A–CO_2]^-/A^-$ ratio of up to a factor of 30 preventing the detection of A^- at slightly elevated voltages (Fig. 12.11) [81].

For NSD it is not required to have a true nozzle–skimmer arrangement. Instead, a potential drop of 20–100 V across a suitable pressure region of any ESI interface design suffices to induce this sort of CID. The Bruker Apollo II interface, for example, features a dual ion funnel setup with the first ion funnel in the rough vacuum of the supersonic expansion plume (≈ 3–4 mbar) and the second ion funnel prior to an RF-only hexapole used to alternatively guide or accumulate ions. Here

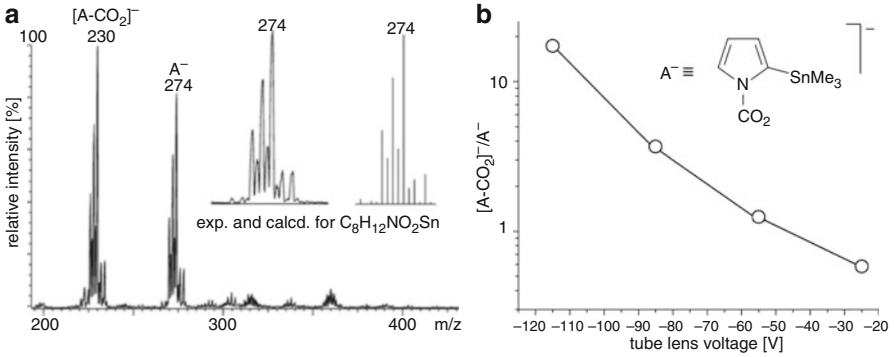

Fig. 12.11 (**a**) Partial negative-ion ESI spectrum of 2-(trismethylstannyl)pyrrole-*N*-carbamate (A^-) from tetrahydrofurane at low nozzle-skimmer voltage drop and (**b**) dependence of the $[A–CO_2]^-/A^-$ ratio variation on this voltage

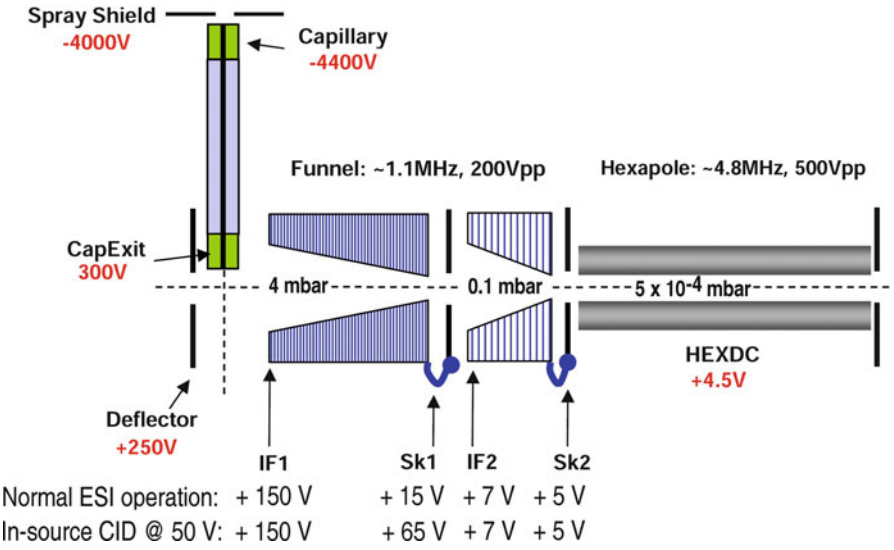

Fig. 12.12 ESI interface with differential pumping in a dual ion funnel arrangement (Bruker Apollo II™). In normal ESI operation the main DC gradient is located in the first ion funnel while ions drop only by about 8 V into the second. Lifting the exit potential of the first funnel causes the ions to enter the second ion funnel at much higher velocity, which is sufficient for NSD (Courtesy of Bruker Daltonik GmbH, Bremen)

NSD or *in-source CID* as it is termed by the manufacturer, is achieved by shifting the DC potentials as to have the largest voltage drop at the entrance into the second ion funnel where a pressure of ≈ 0.1 mbar is suitable for low-energy CID (Fig. 12.12).

12.3 Nanoelectrospray

Miniaturization of electrospray is even more attractive than access to high liquid flows. A more narrow spray capillary results in smaller droplets and, moreover, in much reduced flow, as theoretically described and experimentally demonstrated by Wilm and Mann [82]. Such a downscaling can be achieved by replacing the spray needle by a borosilicate glass capillary of some microliters volume to which a fine tip is pulled with a micropipette puller. The tip has a narrow bore exit of 1–4 µm diameter making flow rates of 20–50 nl min^{-1} sufficient to provide a stable electrospray [83]. Derived from the nanoliter-flow, the term *nanoelectrospray* (nanoESI) has become established for that technique. While conventional ESI produces initial droplets of 1–2 µm in diameter, the droplet size from nanoESI is less than 200 nm, i.e., their volume is about 100–1000 times smaller. NanoESI allows for high-polarity solvents such as pure water in both positive- and negative-ion mode, has extremely low sample consumption [84], and tolerates even higher loads with buffer salts than conventional ESI [55, 85].

Just 800 fmol of BSA consumed In the pioneering nanoESI work, the minuscule sample consumption was demonstrated along an attempt to sequence tryptic peptides (Sect. 11.6.3) of the protein bovine serum albumin (BSA, $M_r \approx 66{,}400$ u). Each of the BSA-derived peptide ions shown in the full scan spectrum (Fig. 12.13) was subjected to fragment ion analysis by means of CID-MS/MS on a triple quadrupole instrument. Merely 800 fmol of BSA was consumed for the tryptic digest used in this analysis [84], a type of nanoESI application that is still highly attractive [86].

12.3.1 Practical Considerations for NanoESI

For the measurement, the nanoESI capillary is adjusted to locate at about 1 mm distance from the entrance of the counter electrode by means of a micromanipulator. Thus, precise optical control is needed during positioning to prevent crashing of the tip or electric discharges during operation. Commercial nanoESI sources are therefore equipped with a built-in microscope or camera (Fig. 12.14). The spray voltage of 0.7–1.2 kV is normally applied via an electrically conducting coating on the outer surface of the spray capillaries, usually a sputtered gold film. Occasionally, wider capillaries with a fine metal filament inside are used. With the high voltage switched on, the liquid sample flow is solely driven by capillary forces refilling the aperture as droplets are leaving the tip. Sometimes, liquid flow is slightly supported by a gentle backing pressure on the capillary. Meanwhile, numerous specialized *nanoelectrospray emitters* – as these capillaries are often termed – have been developed to deliver optimum performance under various conditions of operation including nanoLC-MS coupling [87].

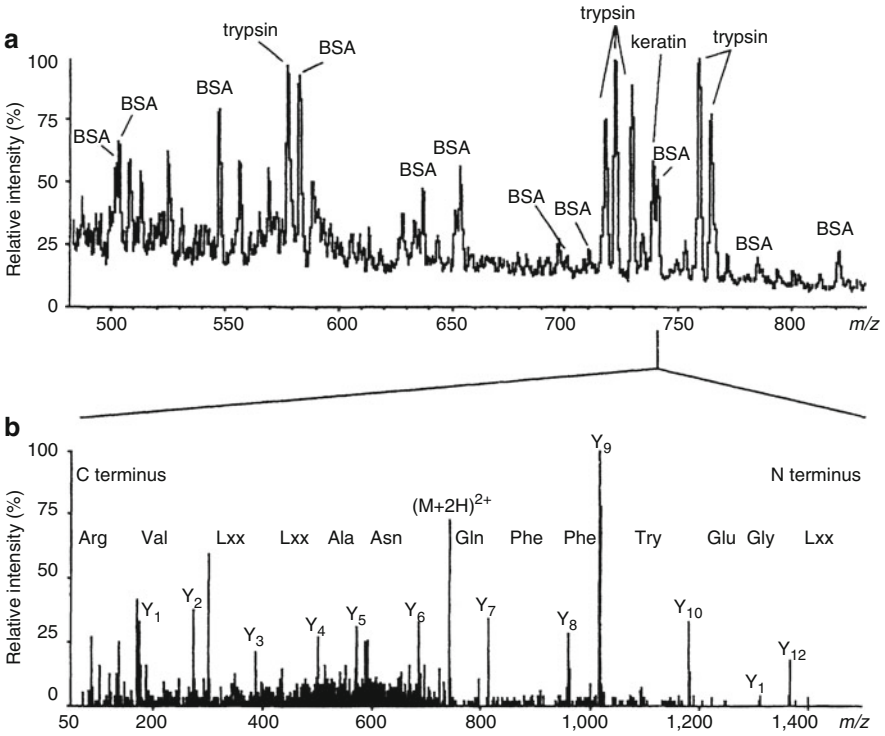

Fig. 12.13 Peptide sequencing by nanoESI-CID-MS/MS from a tryptic digest of BSA; 800 fmol of BSA were used: (**a**) full scan spectrum, (**b**) fragmentation of the selected doubly charged peptide ion at *m*/*z* 740.5 (Adapted from Ref. [84] by permission. © Nature Publishing Group, 1996)

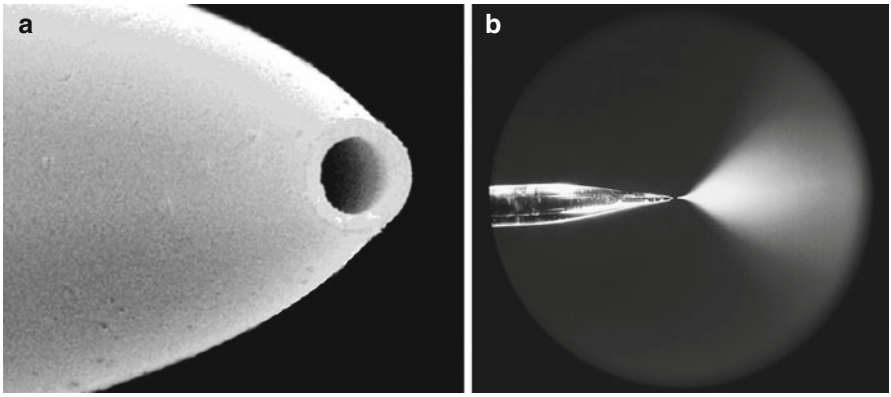

Fig. 12.14 Nanoelectrospray; (**a**) SEM micrograph of the open end of a glass nanoESI capillary having a 2-μm aperture, (**b**) microscopic view of the spray from a nanoESI capillary as provided by observations optics (By courtesy of New Objective, Woburn, MA)

Advantages of nanoESI: Besides its low sample consumption, nanoESI is free of *memory effects* because each sample is supplied in a fresh capillary by means of disposable micropipettes. Furthermore, the narrow exits of nanoESI capillaries prevent air-sensitive samples from rapid decomposition.

12.3.2 Spray Modes of NanoESI

The onset of electrospray as well as the spatial and temporal characteristics of the spray plume largely depends on the experimental parameters. Strong effects are exerted by surface tension and polarity of the solvent, sample concentration, and electric field strength at the tip of the spray capillary. The latter parameter can easily be adjusted, and as demonstrated in Fig. 12.15, demands for careful control as to avoid disadvantageous spray conditions. At low electric field strength some spray will occur, but mostly by multiple discontinuous jets (dripping mode, D) not accompanied by useful aerosol formation [88]. Increasing the spray voltage initiates the formation of the charged mist, which is still accompanied by a spindle-like jet (S) taking away most of the liquid flow. Further increase of the spray voltage forms a wide cone-jet (C) purely consisting of charged microdroplets. As the voltage exceeds a certain limit, the electrostatically driven dissipation of liquid surmounts the solvent flow attainable through the narrow capillary orifice, and thus, the cone-jet starts pulsing (P). Finally, at very high voltages any rough edge around the capillary orifice may initiate a cone-jet of its own. This multi-jet mode

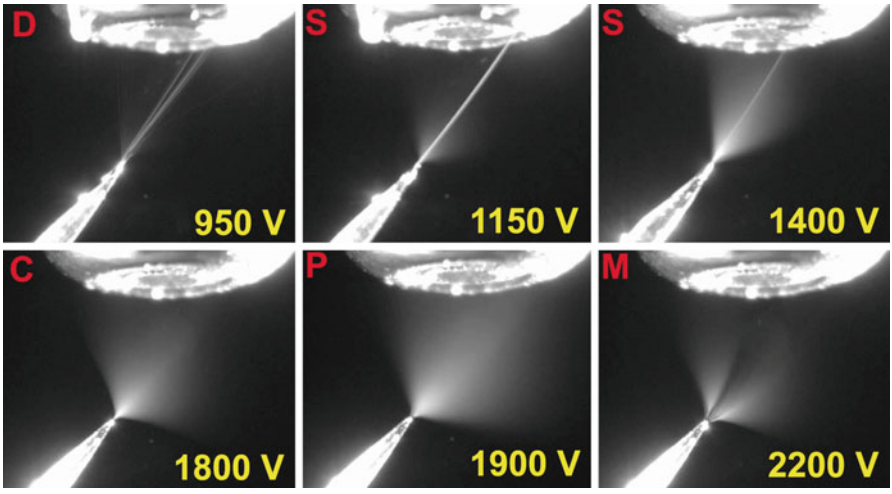

Fig. 12.15 Photographs of nanoelectrospray plumes as effected by different spray voltages. The modes observed starting from the *upper left* are dripping (***D***), spindle (***S***), cone-jet (***C***), pulsed cone-jet (***P***), and multi-jet (***M***). Only pure cone-jet mode will deliver stable electrospray for analytical work (Reproduced from Ref. [88] with permission. © Elsevier, 2004)

(M) causes losses due to overly wide dissipation of the sample flow. Any further increase of the spray voltage results in electric discharges not only detrimental for the capillary tip but eventually also causing failures of the instrument's electronics.

Applicable to ESI in general: These observations are equally relevant to (pneumatically-assisted) ESI at standard flows [89]. Then, the corresponding voltages are just higher by a factor of ≥ 2, which is mostly due to the increased gap between spray capillary and counter electrode to accommodate the larger plume. The optimization of the electrospray for temporal stability by adjustment of liquid flow, nebulizer gas pressure, and spray voltage is therefore necessary for any analytical ESI work.

12.3.3 Nanoelectrospray from a Chip

The sample throughput of nanoESI is limited by the comparatively time-consuming procedure of manual capillary loading. A chip-based nanoESI sprayer on an etched silicon wafer allows for the automated loading of the sprayer array by a pipetting robot (Fig. 12.16). The chip provides a 10×10 array of nanoESI spray nozzles of 10 µm inner diameter. Volumes up to 10 µl are supplied directly from a pipette contacting the chip from the backside. An electrically conducting coating of the pipette tip is used to connect the sprayer to high voltage. Pipetting robot and automated chip handling are united in a common housing that replaces the conventional (nano)ESI spray unit.

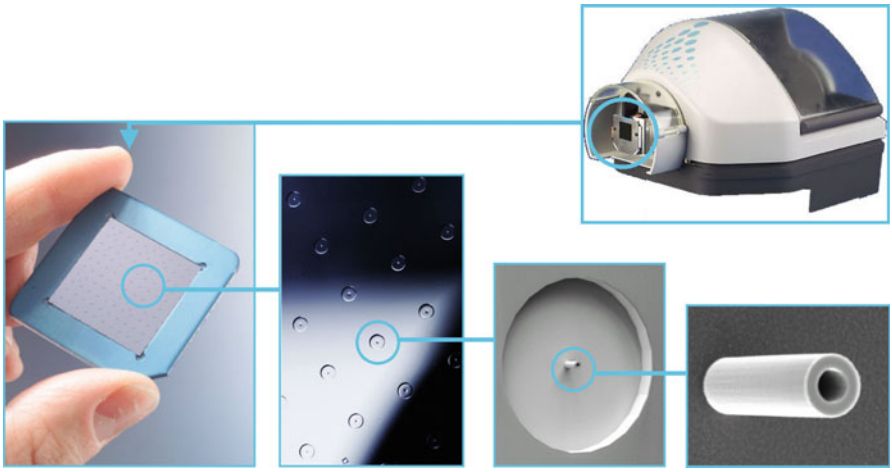

Fig. 12.16 Chip-based Advion nanoESI system. The pictures stepwise zoom in from the pipetting unit to the spray capillary on the silicon chip (By courtesy of G. Schultz, Advion BioSciences, Ithaca, NY)

12.4 Ion Formation in ESI

Until now, our discussion of electrospray was rather technical with an emphasis on interface design and occasional reference to applications. Next we shall consider the physicochemical aspects of the ESI process. This section presents answers to basic questions such as to why an electrospray does occur at all, how isolated gas phase ions are formed from droplets, and what rules are governing the charge state (distribution) of those incipient gas phase ions [89–91]. Ion formation in ESI can be considered to be composed of these steps:

- spraying of a electrostatically charged aerosol of micrometer-sized droplets,
- dramatic reduction of the droplets' size by rapid solvent evaporation,
- repeated disintegration of the microdroplets into even smaller units, and finally
- liberation of fully desolvated ions into the gas phase.

12.4.1 Formation of the Electrospray Plume

To understand the formation of a continuous spray, consider the surface of an electrolytic solution when exiting an electrically conducting capillary held at high electric potential with reference to a nearby counter electrode. In practice, the spray capillary has about 75 μm inner diameter and is kept at 3–4 kV with reference to the sampling orifice at approximately 1 cm distance. At the open end of the capillary the emerging liquid is thus exposed to an electric field of about 10^6 V m^{-1}. The electric field causes charge separation in the electrolytic solution and finally deformation of the meniscus into a cone. The phenomenon of cone formation has been discovered by Zeleny [41] and first theoretically described by Taylor [42], hence it was termed *Taylor cone*.

The process of Taylor cone formation starts when the spherical surface forms an oval under the influence of increasing field strength. In turn, a sharper curvature of the oval increases the field strength. The Taylor cone forms as soon as the critical electric field strength is reached and starts ejecting a fine jet of liquid from its apex towards the counter electrode when surface tension is overcome by the electrostatic forces [82]. The jet carries a large excess of ions of one particular charge sign, because it emerges from the point of highest charge density, i.e., from the cone's apex [92]. Such a jet, however, cannot remain stable for an elongated period of time but breaks up into small droplets (Fig. 12.17) [93]. Due to their charge, these droplets are driven apart by Coulombic repulsion. Overall, this process causes the generation of a fine spray, and thus gave rise to the term *electrospray* (Figs. 12.18). This mode of operation is termed *cone-jet mode* [6].

The ESI process overall represents an electrolytic flow cell where the connection from the spray capillary to the counter electrode is created by charge transportation via the electrically charged aerosol (Fig. 12.19) [94–96]. In positive-ion mode,

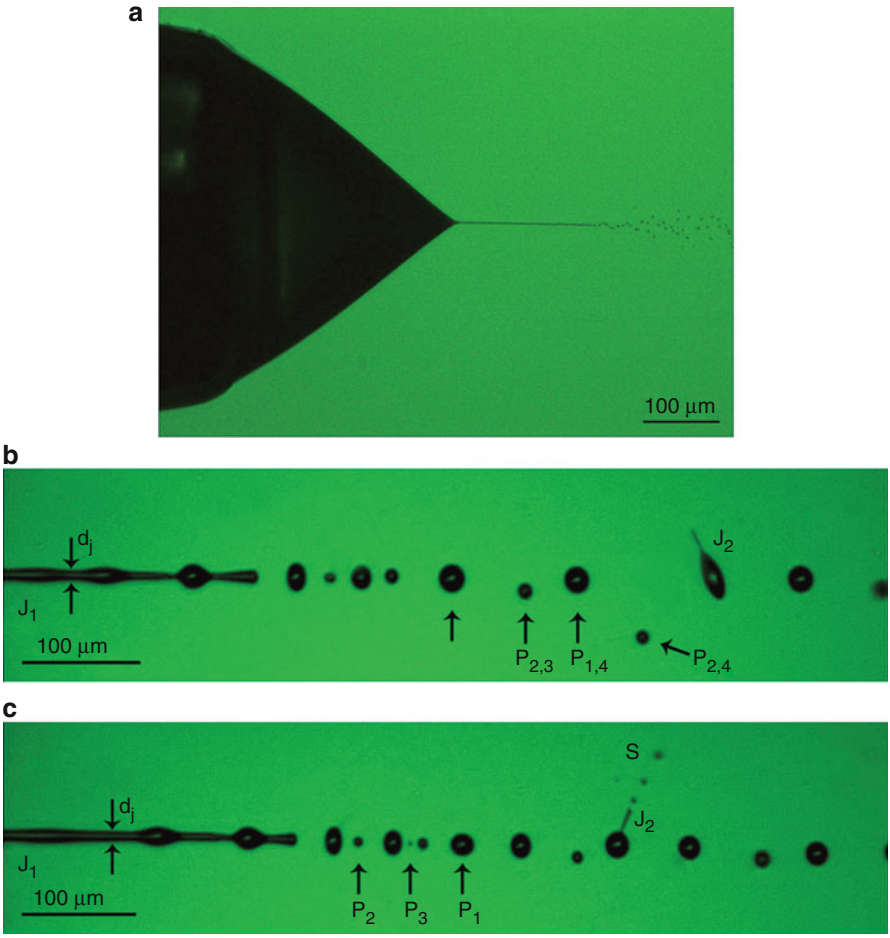

Fig. 12.17 Taylor cone and jet disintegration in ESI. (**a**) Microphotograph of the meniscus shape during electrospray in stable cone-jet mode for optimum analytical operation. The shape and the emerging jet remain stationary and continuously delivering numerous small droplets upon breaking up of the jet. Snapshots (**b**, **c**) show details of the transition from jet to droplets and their shrinking by ejection of a series of much smaller off-spring droplets (Adapted from Ref. [93] with permission. © American Chemical Society, 2007)

neutralization at the sampling orifice is effected by electrons from the high voltage power supply, which in turn originate from oxidation of anions on the inner wall of the spray capillary. In negative-ion mode, reduction of cations will occur in place of oxidation [64].

$M^{+\bullet}$ ions in ESI mode? Under rare circumstances, in ESI, molecular ions, $M^{+\bullet}$, can be formed. This requires that the electrolytic processes during electrospray cause molecular ion formation by electrolytic oxidation [96]. An electrolytic

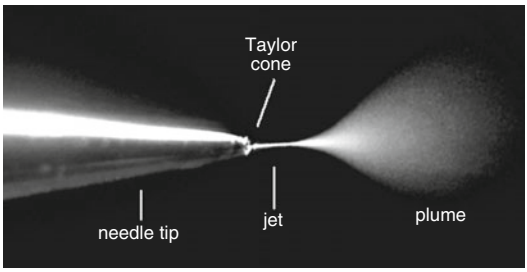

Fig. 12.18 Electrospray from a nanoESI capillary. The jet emitted from the Taylor cone is clearly visible and separate from the region of rapid expansion into a plume of microdroplets (By courtesy of New Objective, Woburn, MA)

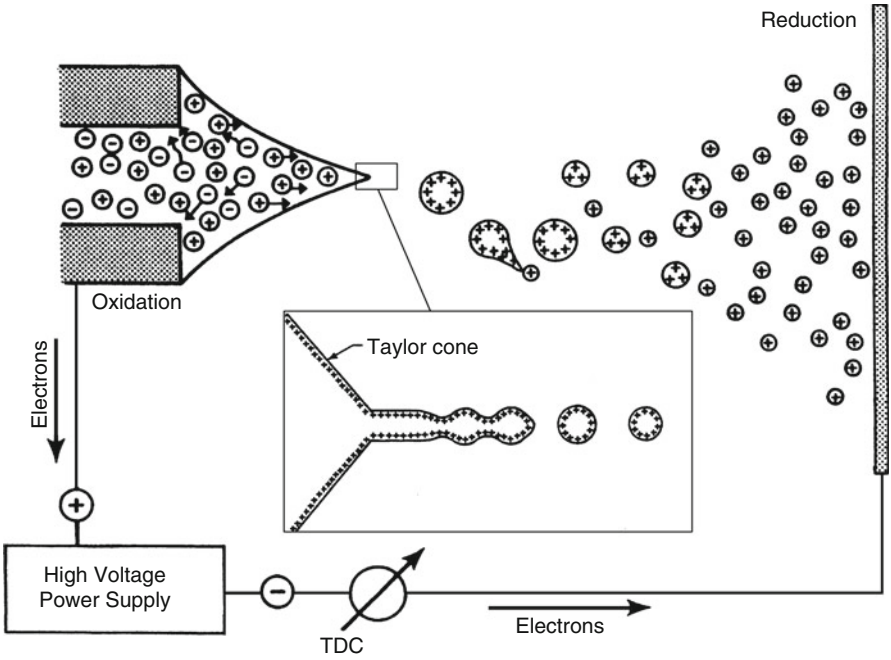

Fig. 12.19 Schematic of Taylor cone formation, ejection of a jet, and its disintegration into a fine spray. The electrochemical processes of ESI [94, 95] are also assigned (Adapted from Ref. [54] by permission of the authors)

molecular ion formation becomes more probable if nonpolar molecules of very low ionization energy are precluded from other ionization pathways such as protonation or cationization. Electrolytic $M^{+\bullet}$ ion formation normally requires perfectly dry aprotic solvents, low liquid flow for increased reaction time, and preferably metal spray capillaries rather than fused silica capillaries. ESI may also result in changes of the oxidation state of metal ions, e.g., $Ag^{+} \rightarrow Ag^{0}$, $Cu^{2+} \rightarrow Cu^{+}$.

12.4.2 Disintegration of Charged Droplets

When a micrometer-sized droplet carrying a large excess of ions of one particular charge sign – some 10^4 charges can be considered to be a realistic value – evaporates some solvent, the charge density on its surface is continuously increased. As soon as electrostatic repulsion exceeds the conservative force of surface tension, disintegration of the droplet into smaller subunits will occur. The point at which this occurs is known as the *Rayleigh limit* [43]. Originally, it has been assumed that the droplets would then be degraded by *Coulomb fission* (or *Coulomb explosion*). This process then occurs repeatedly to generate increasingly smaller microdoplets. While the model of a cascading reduction in size holds valid, more recent work has demonstrated that the microdroplets do not explode, but eject a series of much smaller microdroplets from an elongated end (Figs. 12.17, 12.19, and 12.20) [54, 90, 93, 97]. The ejection from an elongated end can be explained by deformation of the flying microdroplets, i.e., they have no perfect spherical shape. Thus, the charge density on their surface is not homogeneous, but significantly increased in the region of sharper curvature. The smaller offspring droplets carry off only about 1–2% of the mass, but 10–18% of the charge of the parent droplet [90]. This process resembles the initial ejection of a jet from the Taylor cone. The concept of this so-called *droplet jet fission* is not only based on theoretical considerations but has been proven by flash microphotographs of droplet

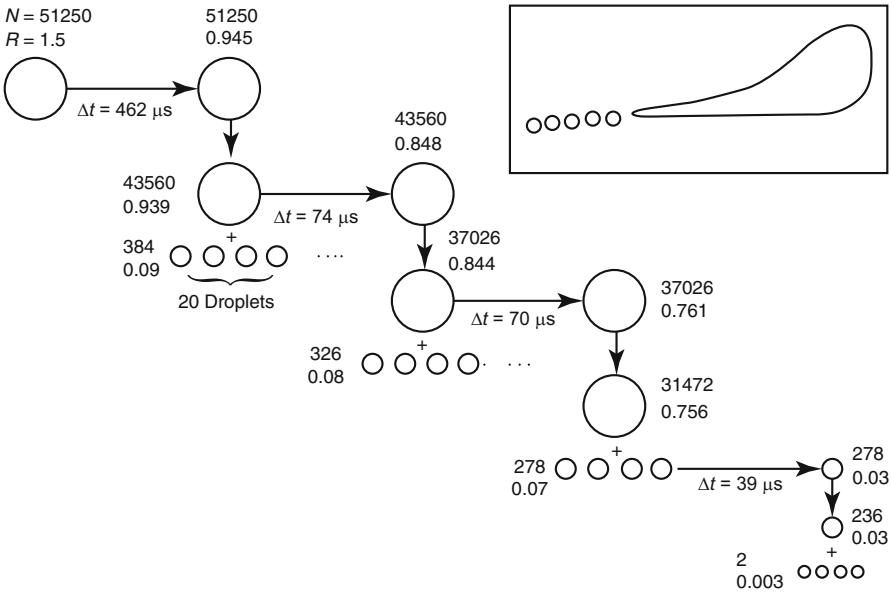

Fig. 12.20 Droplet jet fission. The average number of charges on a droplet, the radii of the droplets [μm], and the timescale of events are assigned. The *inset* shows a drawing of droplet jet fission based on an actual flash microphotograph published by Gomez and Tang [97] (Reproduced from Ref. [54] by permission of the authors)

shadows [97, 98]. The total series of events from the initially sprayed droplet to the isolated ion takes less than one millisecond. Micro-shadowgraphs also show that neutral droplets exhibit an analogous distortion of their shapes followed by ejection of off-spring droplets when field ionized by an electric field of about 2.5×10^6 V m^{-1} [99].

12.4.3 Formation of Gas-Phase Ions from Charged Droplets

The process of droplet jet fission starts on a macroscopic scale and eventually leads to states that might be regarded as large clusters or multiply solvated ions. This model does not address the final step of the creation of isolated gas phase ions from these multi-molecular entities, however.

The elder model of ion formation, the *charged-residue model* (CRM), assumes complete desolvation of ions to occur by successive loss of all solvent molecules from droplets that are sufficiently small to contain just one analyte molecule at the end of a droplet fission cascade [22, 47, 100]. The charges, e.g., protons, being part of this ultimate droplet are then transferred onto the (macro)molecule, especially if this exposes some basic sites. According to CRM, even large proteins should at least be able to form singly charged ions, although the formation of multiply charged species should be of higher probability. In fact, all charge states down to 1+ have been observed [27].

A later theory, the *ion evaporation model* (IEM) [101, 102], describes the formation of desolvated ions as direct evaporation from the surface of highly charged microdroplets [103] (for ion evaporation in FD-MS cf. Sect. 8.6). Ionic solvation energies are in the range of 3–6 eV, but at 300 K thermal energy can only contribute about 0.03 eV to their escape from solution. Thus, the electric force has to provide the energy needed. It has been calculated that a field of 10^9 V m^{-1} is required for ion evaporation, which corresponds to a final droplet diameter of 10 nm [102]. The IEM nicely corresponds to the observation that the number of charges is related to the fraction of the microdroplet's surface that a (macro)molecule can cover. Upon shrinking of the droplet, the size of such a molecule and number of droplet charges remain constant. Now, the increasing charge density brings more charges within the reach of an analyte molecule as the spacing of the surface charges decreases [104, 105]. Flat and planar molecules therefore exhibit higher average charge states than compact ones, e.g., the unfolding of (globular) proteins is accompanied by higher charge states under otherwise identical ESI conditions [106, 107].

Further support of IEM comes from the effect of the droplet evaporation rate on the charge state distribution of proteins. Fast evaporation (more drying gas, higher temperature) favors higher average charge states, while slower evaporation results in fewer charges. This is in accordance with the reduced time available for ion evaporation from the shrinking droplet. It leads to a relative enrichment of charge on the droplet, and thus, on the leaving ions [104].

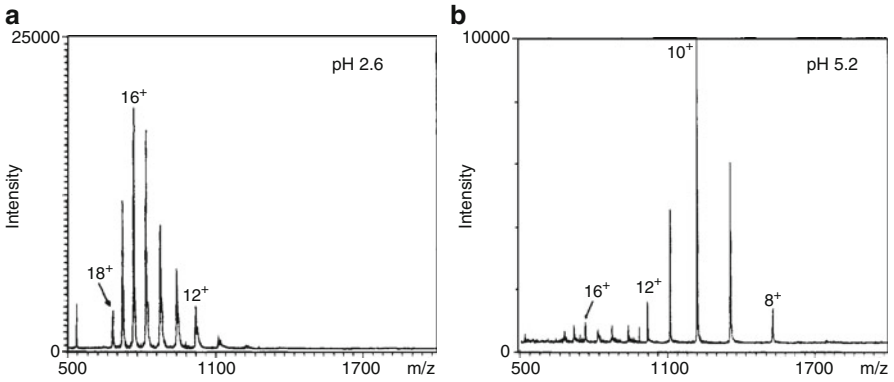

Fig. 12.21 Positive-ion ESI mass spectra of cytochrome c at different pH of the sprayed solution: (**a**) at pH 2.6, (**b**) at pH 5.2 (Adapted from Ref. [107] by permission. © American Chemical Society, 1990)

Influencing the charge state by pH The average charge state of a protein depends on whether it is denatured or not and on the actual solvent; lower pH causes more protons to be attached to the protein than neutral conditions [107, 108]. The degree of denaturization in turn depends on the pH of the electrosprayed solution. Resulting conformational changes of the protein, e.g., unfolding upon protonation, make additional basic sites accessible, thereby effecting an increase of the average charge state (Fig. 12.21) [107]. The maximum number of charges that can be placed upon peptide and protein molecules is directly related to the number of basic amino acid residues (arginine, lysine, histidine) present.

Influencing the charge state by reduction The cleavage of disulfide bonds by reduction with 1,4-dithiothreitol causes the unfolding of the protein. This exposes additional basic sites to protonation, and therefore results in higher average charge states in the corresponding positive-ion ESI spectrum (Figs. 12.22 and 12.23) [106].

In contradiction to IEM, the electric field strength locally necessary to evaporate ions from a droplet cannot be attained, because the droplet would be crossing the Rayleigh limit before [27, 109].

Other work revealed the importance of gas-phase proton transfer reactions [110–113]. This implies that multiply charged peptide ions do not exist as preformed ions in solution, but are generated by gas-phase ion–ion reactions. The proton exchange is driven by the difference in proton affinities (*PA*, Sects. 2.12 and 9.17) of the species encountered, e.g., a protonated solvent molecule of low *PA* will protonate a peptide ion with some basic sites left. Under equilibrium conditions, the process would continue until the peptide ion is "saturated" with protons, a state that also marks its maximum number of charges.

Even though the pathways of ion formation in ESI may be debatable [90, 91, 105], we can briefly summarize this as follows: CRM can be assumed to hold valid for large molecules [22], while the formation of smaller ions is better described by IEM [90, 91].

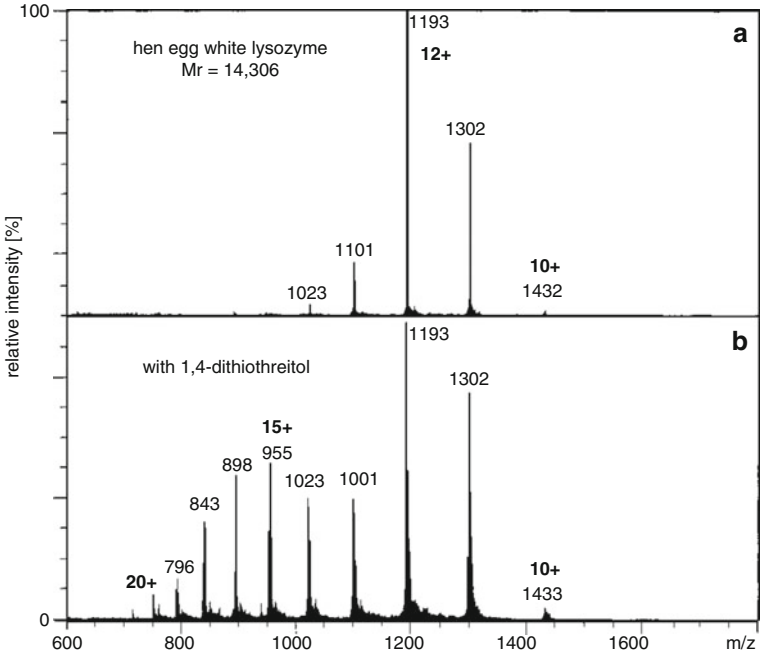

Fig. 12.22 Positive-ion ESI spectra of (**a**) hen egg white lysozyme and (**b**) the protein after addition of 1,4-dithiothreitol (Reproduced from Ref. [106] by permission. © American Chemical Society, 1990)

Independent of the "true" mechanism of ion liberation, the close correlation between the numbers of charge states and the surface a macromolecule exposes to its surrounding solvent can be used to observe these changes by ESI-MS [106–108, 114, 115].

12.5 Multiply Charged Ions and Charge Deconvolution

12.5.1 Dealing with Multiply Charged Ions

The above discussion of ion formation in ESI has revealed that – apart from compound class – the actual experimental conditions exert significant influence on the appearance of an ESI spectrum. The most influential factors are:

- pH of the sprayed solution,
- flow of sample solution,
- flow (or pressure) of nebulizing gas, and
- flow and temperature of the desolvation gas or the temperature of the heated desolvation capillary, respectively.

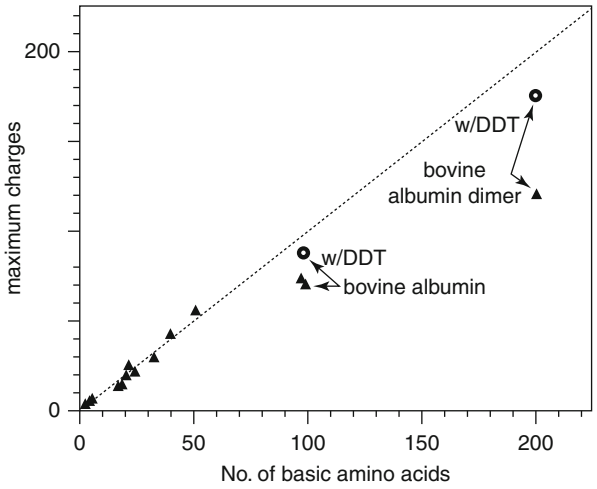

Fig. 12.23 Correlation between the number of basic amino acid residues and the maximum number of charges observed for a set of peptides and proteins under ESI conditions. Labels w/DDT indicate reduction with dithiothreitol in solution (Reproduced from Ref. [106] by permission. © American Chemical Society, 1990)

In ESI, the number of charges on a molecule basically depends on its molecular weight [22, 116] and on the number of potential charge sites available, e.g., sites for protonation [12, 22, 106, 107], deprotonation [117, 118], or cationization [119]. On the one hand, this behavior advantageously folds up the m/z scale to make even extremely large molecules accessible to standard mass analyzers, e.g., up to m/z 3000 (Fig. 12.24). On the other hand, it creates a confusingly large number of peaks and requires tools to deal with in order to enable reliable mass assignments of unknown samples.

While low-mass polymers exhibit only singly charged ions in ESI, polymers of higher mass form doubly, triply, and multiply charged ions [16]. Basically, the number of charges on those molecules increases in parallel to their average molecular weight. For example, polyethylene glycol of an average molecular mass of 400 u (PEG 400) exclusively exhibits singly charged ions in positive-ion ESI. PEG 1000 about equally forms 1+ and 2+ charge states, and with PEG 1500 the 3+ charge state starts to dominate [16, 105].

Furthermore, charge distributions depend on the sample concentration, e.g., PEG 1450 yields triply and few doubly charged ions at 0.005 mg ml^{-1} in MeOH : H_2O = 1 : 1, triply and doubly charged ions of equal abundance plus few singly charged ions at 0.05 mg ml^{-1}, but mainly doubly charged ions accompanied by few singly and triply charged ions at 0.5 mg ml^{-1} [105]. This demonstrates that a comparatively fixed number of charges in a droplet is distributed among few or many analyte molecules contained, and thus, supports IEM.

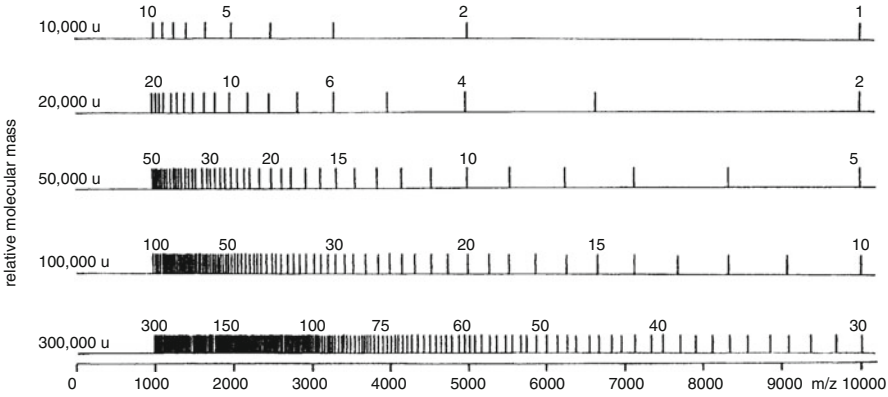

Fig. 12.24 Calculated *m*/*z* values for the different charge states of molecules of different molecular weight. Representative peaks are labeled with their corresponding charge state (Adapted from Ref. [116] by permission. © John Wiley & Sons, 1992)

Multiple cationization of PEG PEGs and related oxygen-rich compounds readily form $[M+alkali_n]^{n+}$ ions [16, 119, 120] or $[M+n NH_4]^{n+}$ ions. Triton X-405, a commercial detergent used in acrylic paints for stabilization of the suspension, has been analyzed by positive-ion nanoESI-MS. The molecular weight distribution appeared trifold; in this case, due to the presence of ammonium acetate as $[M+NH_4]^+$, $[M+2NH_4]^{2+}$, and $[M+3NH_4]^{3+}$ ion series (Fig. 12.25a). For endgroup analysis *nozzle-skimmer dissociation* (NSD) was applied at 60 V offset upon which only the $[M+3NH_4]^{3+}$ ions (least stable due to highest internal Coulombic repulsion) underwent significant dissociation to yield some low-mass fragment ions (Fig. 12.25b). The occurrence of $[C_8H_{17}\text{-}C_6H_4\text{-}(OC_2H_4)_n]^+$ ions at *m*/*z* 233 and 277 pointed towards octylphenyl endgroups. Their presence was then verified in a pseudo MS^3 experiment by CID-MS/MS of the fragment ion at *m*/*z* 233 at 20 V collision offset (Fig. 12.25c) [79].

Annoying superimposition: In ESI spectra of (synthetic) polymers, multiple charging causes the simultaneous occurrence of superimposing ion series each of them representing the molecular weight distribution of the polymer. Therefore, MALDI (Chap. 11) is generally preferred for polymer analysis as it delivers only singly charged ions, and thus provides mass spectra that are much easier to interpret.

12.5.2 Mathematical Charge Deconvolution

How would we be able to retrieve the correct molecular weight from ESI spectra as just presented in Figs. 12.21 and 12.22, or even worse, at the beginning of this chapter, in Fig. 12.1, if the charge states corresponding to individual peaks were not yet assigned? A systematic treatment of these ion series reveals that adjacent signal groups (to include isotopic patterns) in an ESI mass spectrum of a pure compound

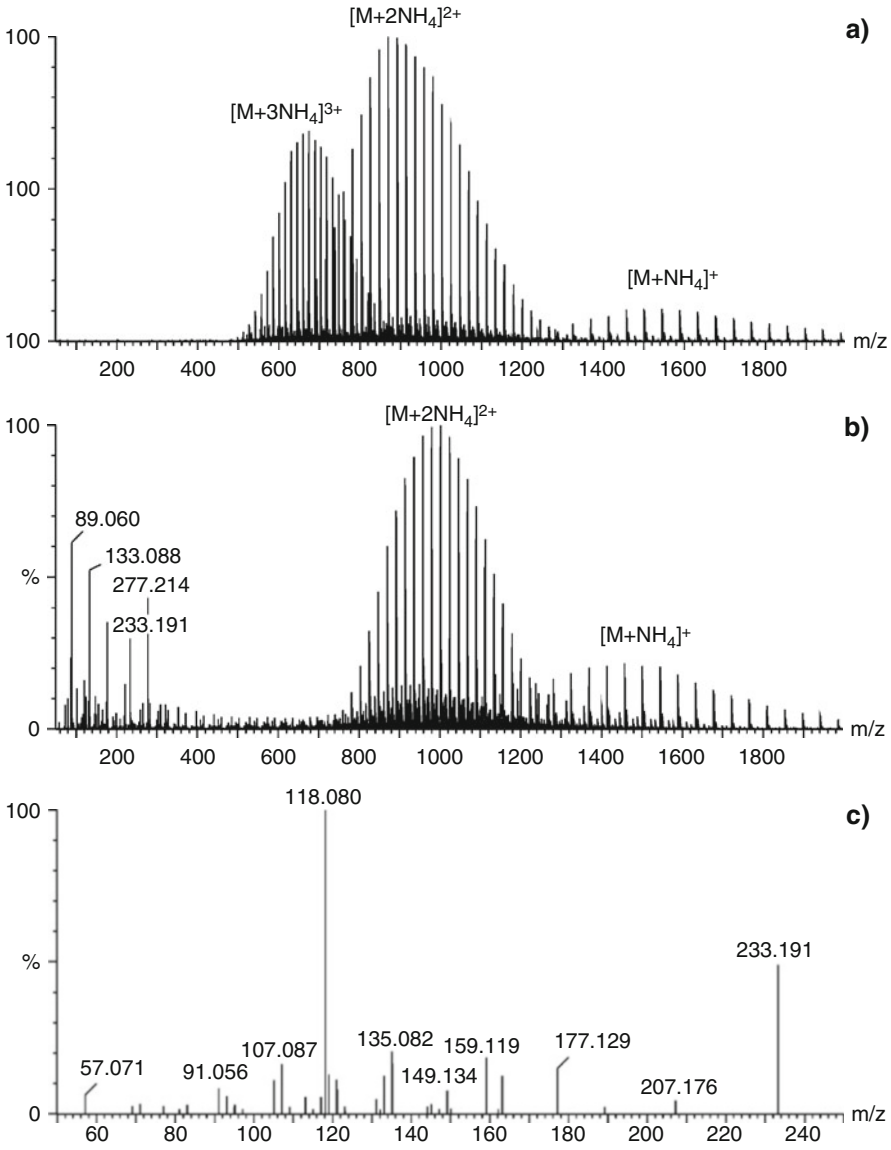

Fig. 12.25 Triton X-405 analyzed by positive-ion nanoESI-MS. (**a**) Molecular weight distribution appears trifold as $[M+NH_4]^+$, $[M+2NH_4]^{2+}$, and $[M+3NH_4]^{3+}$ ions series; (**b**) only the triply charged ions undergo significant dissociation upon NSD to yield low-mass fragment ions; (**c**) CID spectrum of fragment ion at *m*/*z* 233 for endgroup analysis (Reproduced from Ref. [79] with permission. © Elsevier, 2009)

belong to charge states differing exactly by one, i.e., distributions have no gaps or jumps. This renders the calculation of the number of charges corresponding to individual peaks straightforward, and thus, permits to deduce an unknown molecular weight M_r [63, 116, 121].

For the charge states of neighboring peaks belonging to a pair at m/z_1 (higher value) and m/z_2 (lower value) we have :

$$n_2 = n_1 + 1 \tag{12.1}$$

Assuming all charges from protonation and using m_H for the mass of a proton, m/z_1 is determined by

$$m/z_1 = \frac{M_r + n_1 m_H}{n_1} \tag{12.2}$$

and m/z_2 of the peak at lower mass is given by

$$m/z_2 = \frac{M_r + n_2 m_H}{n_2} = \frac{M_r + (n_1 + 1)\, m_H}{n_1 + 1} \tag{12.3}$$

where n_2 can be expressed by inserting Eq. 12.1. The charge state n_1 can then be obtained from

$$n_1 = \frac{m/z_2 - m_H}{m/z_1 - m/z_2} \tag{12.4}$$

Having calculated n_1, M_r is given by

$$M_r = n_1\,(m/z_1 - m_H) \tag{12.5}$$

In case of cationization instead of protonation, m_H has to be replaced by the corresponding mass of the cationizing agent, in most cases simply by that of NH_4^+, Na^+, or K^+. (The recognition of cationized species is addressed in Sects. 8.6 and 11.4).

Manual charge deconvolution For the ease of calculation we use nominal mass (Sect. 3.1.5) and assume the charges from protonation. Consider the first peak at m/z 1001, the second at m/z 501. Now n_1 is obtained according to Eq. 12.4 from $n_1 = (501 - 1)/(1001 - 501) = 500/500 = 1$. Therefore, M_r is calculated from Eq. 12.5 to be $M_r = 1 \times (1001 - 1) = 1000$. (The doubly protonated ion is detected at m/z 501 because (1000 + 2)/2 = 501.)

Averaging increases accuracy: As each pair of signals delivers an independent mass value for the hypothetical singly charged ion, mass accuracy can greatly be enhanced in ESI by multiple determination of this value and subsequent calculation of the average.

12.5.3 Computerized Charge Deconvolution

The above procedure may be time-consuming but at least it works for pure compounds. When mixtures are to be addressed, proper manual assignment of all peaks becomes increasingly difficult. Additional problems arise from the simultaneous presence of peaks due to protonation and cation attachment. Therefore, numerous refined algorithms have been developed to cope with these requirements [122–125]. Modern ESI instruments normally come with elaborate *charge deconvolution* software or offer such software as an option. The efficiency of these programs [126–128] can largely be improved by specifying some limitations, e.g., the expected range of charge numbers, the type of ions or presumed adducts, and the resolving power employed for the measurement. The resolving power is relevant to assist the algorithm in distinguishing neighboring peaks of other charge states from isotopic contributions.

ESI-MS of transferrin Transferrin, a human protein of close to 80 kDa, occurs in several glycoforms, i.e., its structure contains different antenna-shaped oligosaccharide receptors. Here, these are indicated by labels for one biantenna (Bi), two biantennas (BiBi), one biantenna plus one triantenna (BiTri), and one biantenna plus one fucosylated biantenna (BiBiF), respectively. Transferrin may also lack an *N*-glycan, even in healthy individuals, while truncated transferrin, indicated by X and Y, may occur due to inappropriate storage or handling. The positive-ion ESI mass spectrum of transferrin from a healthy individual was measured using a medium-resolution TOF mass spectrometer (QSTAR, AB Sciex). The spectrum was obtained of a solution in acetonitrile : water = 60 : 40 (v/v) with 0.1% of formic acid. Under these conditions, multiple protonation leads to a wide distribution of charge states, mainly covering the range m/z 1700–3000 (Fig. 12.26) [129]. However, it is hardly possible to detect all components contributing to the spectrum without charge deconvolution. After using ProMass deconvolution software (Thermo Fisher Scientific) to transform the raw data into a spectrum reflecting only singly charged ions, the individual components are easily recognized. The contributing proteins detected are X (69022 u), Y (73430 u), Bi (77363 u), BiBi (79553 u), BiBiF (79769 u), and BiTri (80205 u).

ESI-MS at different levels of resolution A mixture of the proteins bovine ubiquitin, horse cytochrome c, and horse myoglobin, each at a concentration of 10 µM, was analyzed by positive-ion ESI-FT-ICR-MS. While the first analysis was carried out with only 16 k data (LR), the second was obtained from a 512 k transient (HR), resulting in $R = 2000$ and $R = 60{,}000$, respectively (Sect. 4.7.5). Charge deconvolution by the *Zscore* algorithm delivered "zero-charge spectra" clearly separating the proteins (Fig. 12.27) [123]. The program used here handles LR spectra to yield unresolved isotopic distribution envelopes as well as HR spectra to show the full isotopic information in the resulting zero-charge spectrum.

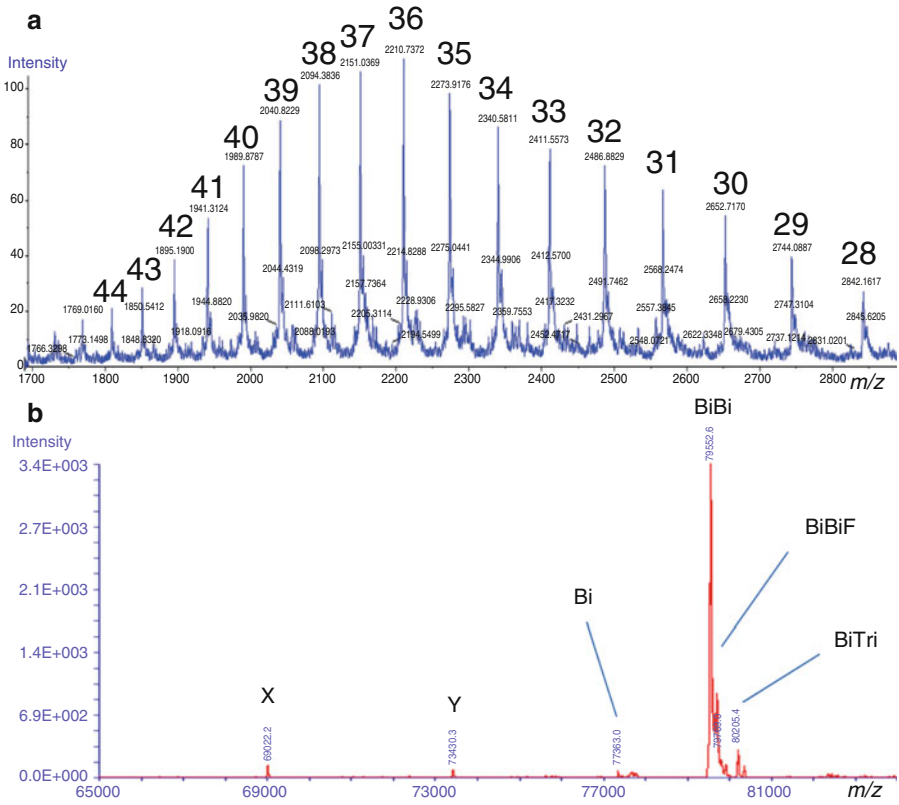

Fig. 12.26 Positive-ion ESI mass spectrum of a solution of transferrin in acetonitrile : water = 60 : 40 (v/v) with 0.1% of formic acid. (**a**) Spectrum as measured with the number of charges assigned, (**b**) after charge deconvolution to deliver a hypothetical spectrum of singly charged ions. Labels indicate one biantenna (*Bi*), two biantennas (*BiBi*), one biantenna plus one triantenna (*BiTri*), and one biantenna plus one fucosylated biantenna (*BiBiF*), respectively. Truncated transferrin is indicated by X and Y (Adapted from Ref. [129] with permission. © Springer, 2016)

Charge deconvoluted spectra: The output of computerized charge deconvolution can often be customized to either display the hypothetical mass spectrum as it would appear with singly charged ions (Fig. 12.26) or to deliver "zero-charge" spectra showing the molecular weights of the corresponding neutrals (Fig. 12.27). It is important to note that the output of neutral M_r represents the only case where the abscissa *has to be* labeled "*mass* [u]", while mass spectra strictly require "*m*/*z*" on the *x* axis!

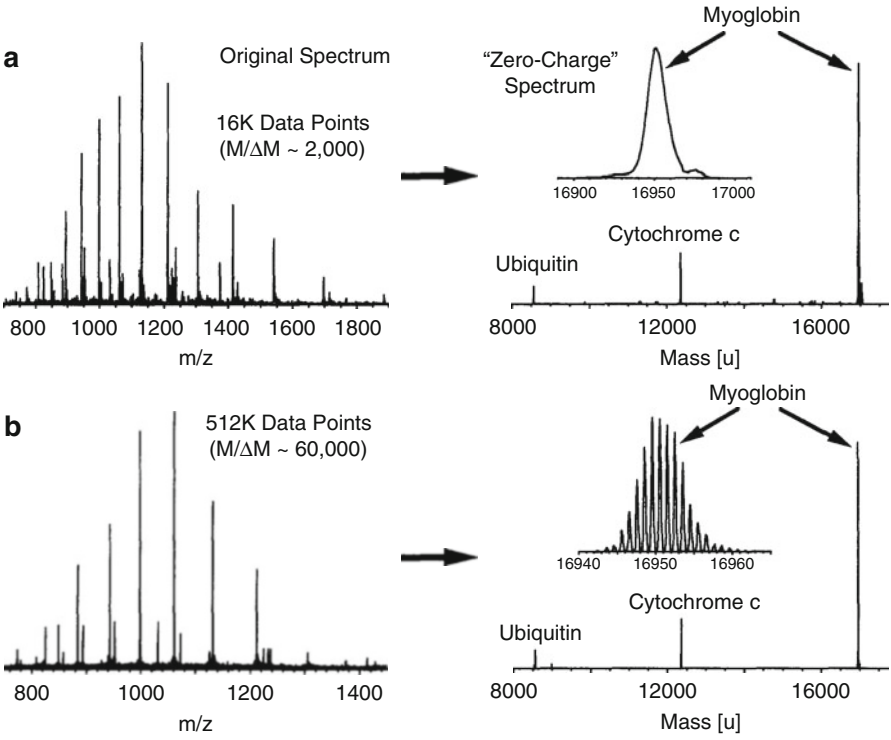

Fig. 12.27 Charge deconvolution of (**a**) LR and (**b**) HR positive-ion ESI spectra of an artificial protein mixture. The "zero-charge" peak of myoglobin is also shown in expanded view to reveal the delineation of the isotopic pattern (Adapted from Ref. [123] by permission. © Elsevier, 1998)

12.5.4 Hardware Charge Deconvolution

The most effective technique to achieve charge deconvolution of complex spectra due to multiply charged ions is to achieve the full separation between signals corresponding to different charge states and to resolve their isotopic patterns. Beyond a molecular weight of about a few thousand u this requires high-resolving mass analyzers, because the isotopic distribution of organic ions then becomes several mass units wide (Fig. 12.28). The minimum resolving power needed for full isotopic separation is always equal to the ion's mass number (Sects. 3.4, 3.7, and 3.8), independent of the charge state of the ion. Lower resolution only envelops the isotopic distribution. At insufficient resolution, the resulting peak may even be wider than the envelope [116].

Magnetic sector instruments (Sect. 4.3) were used first to demonstrate the beneficial effects of high resolution on ESI spectra of biomolecules [120, 130, 131]. Today, FT-ICR instruments (Sect. 4.7) [132, 133] and more recently orthogonal acceleration time-of-flight (oaTOF, Sects. 4.2.8 and 4.9) or Orbitrap (Sect. 4.8) analyzers offer by far more effective means to resolve such signals.

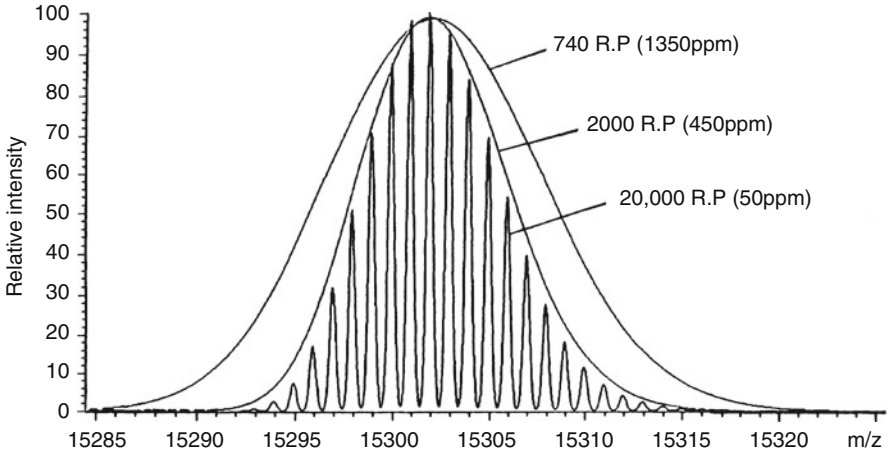

Fig. 12.28 Theoretical peak shape for a hypothetical singly charged protein ion of $M_r = 15{,}300$ u at different settings of resolution (Reproduced from Ref. [116] by permission. © John Wiley & Sons, 1992)

Rule for minimum resolving power: The mass resolving power to achieve full separation of isotopic peaks only depends on the molecular weight, M_r, of the analyte, but it is independent of the number of charges, z, of the ions. For example, the isotope peaks of the $[M+H]^+$ ion of thioredoxin (Fig. 12.1) would appear at m/z 11674 and be spaced at $\Delta(m/z) = 1$. Using $R = m/\Delta m$ (Sect. 3.4) we calculate the minimum value $R_{min} = 11674 / 1 = 11674$. For the $[M+8H]^{8+}$ ion of this protein ($z = 8$), the signals are centered at m/z 1459 and spaced at $\Delta(m/z) = 0.125$. Thus, we calculate $R_{min} = m/\Delta m = 1459 / 0.125 = 11674$. In brief, the numerical value of M_r directly reflects R_{min}.

ESI-Orbitrap mass spectra of intact proteins The positive-ion ESI-Orbitrap mass spectra of intact proteins show fully resolved isotopic patterns when 100 transients at a resolving power setting of $R = 100{,}000$ are acquired and charge deconvoluted. Figure 12.29 shows the results for the $[M+10H]^{10+}$ ion of horse heart apomyoglobin, $m = 16{,}940.965$ u (neutral mass of monoisotopic molecule) and of the $[M+21H]^{21+}$ ion of carbonic anhydrase, $m = 29{,}006.683$ u, both in very good agreement with the calculated isotopic patterns and masses [134]. A comparison with the previous example also demonstrates the great advances made in MS instrumentation that now allows to routinely resolve such signals. (Further examples are given by the ESI-ECD-FT-ICR spectra of proteins in Sect. 9.13 or by example II in the preceding Sect. 12.5.3.)

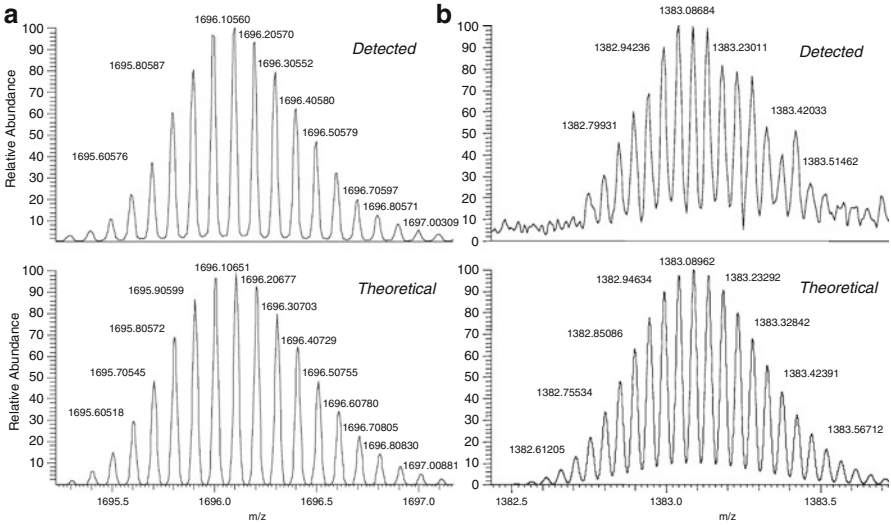

Fig. 12.29 ESI-orbitrap-MS of proteins. Fully resolved isotopic patterns as obtained upon charge deconvolution of (**a**) the $[M+10H]^{10+}$ ion of horse heart apomyoglobin, $m = 16{,}940.965$ u (neutral mass of monoisotopic molecule) and (**b**) the $[M+21H]^{21+}$ ion of carbonic anhydrase, $m = 29{,}006.683$ u (Reproduced from Ref. [134] by permission. © American Chemical Society, 2006)

12.5.5 Controlled Charge Reduction in ESI

The complexity of ESI spectra of mixtures with all components forming series of multiply charged ions is apparent. An alternative approach to high resolution and data reduction by charge deconvolution is presented by the controlled reduction of the charge states themselves. *Charge reduction electrospray* results in a significantly reduced number of peaks per component at the cost of their detection being required at substantially higher m/z [135, 136]. In particular oaTOF analyzers provide a sufficient mass range for such an experimental approach at reasonable cost.

Charge reduction can be accomplished by neutralizing ion–molecule reactions during the desolvation step of ESI. The reducing ions needed for such neutralizations can either be generated by irradiating the gas with a ^{210}Po α-particle source [135, 137] or much more conveniently by a corona discharge [138, 139]. Besides being nonradiative, the corona discharge offers the advantage of being tunable to achieve varying degrees of neutralization (Fig. 12.30) [138, 139].

Ion–ion chemistry of oppositely charged ions provides another access to charge reduction and charge state determination [110]. Such studies were done either by employing the region preceding the skimmer of an ESI interface as a flow reactor or inside a quadrupole ion trap. In the first case, both the substrate ion and the oppositely charged reactant ion are created by means of two separate ESI sprayers attached to a common interface [140]. The approach in a quadrupole ion trap makes

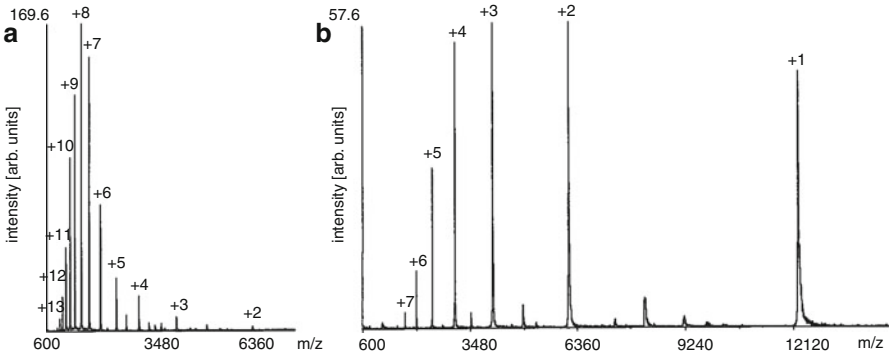

Fig. 12.30 Positive-ion ESI mass spectra of cytochrome c (**a**) under standard ESI conditions from acidic solution, (**b**) same but with medium setting of charge-reducing corona discharge (Adapted from Ref. [138] by permission. © American Chemical Society, 2000)

use of the in-trap generation of proton-transferring reactant ions, while substrate ions are admitted via the ESI interface [141]. Finally, a noninstrumental approach is to derivatize the analytes as to reduce their ability of binding protons at basic functional groups [136].

12.6 Applications of ESI-MS

ESI-MS is not only a versatile tool for any aspects of peptide and protein characterization including their complete sequencing, it also offers a tremendous variety of other applications some of which are highlighted below [4, 9–11, 25, 142–145].

12.6.1 ESI-MS of Small Molecules

Polar analytes in the *m*/*z* 100–1500 range are often involved in pharmaceutical analytics including metabolism studies. The types of ions formed are various and depend on the ion polarity, the pH of the solution, the presence of salts, and the concentration of the sprayed solution. Multiply charged ions are rarely observed.

Drug development The compound below represents the functional part of an effective drug (BM 50.0341) inhibiting HIV-1 infection by suppression of the unfolding of the gp120 glycoprotein (Fig. 12.31). Its positive-ion nanoESI spectrum from ethanol in the presence of ammonium chloride exhibits signals due to the formation of $[M+H]^+$, $[M+NH_4]^+$, and $[M+Na]^+$ ions. In addition, cluster ions of the type $[2M+H]^+$, $[2M+NH_4]^+$, and $[2M+Na]^+$ are observed as typical for samples at comparatively high concentration. In negative-ion mode [146–149], the $[M–H]^-$ ion is accompanied by $[M+Cl]^-$ and $[M+EtO]^-$ adduct ions; the corresponding cluster ion series is also observed.

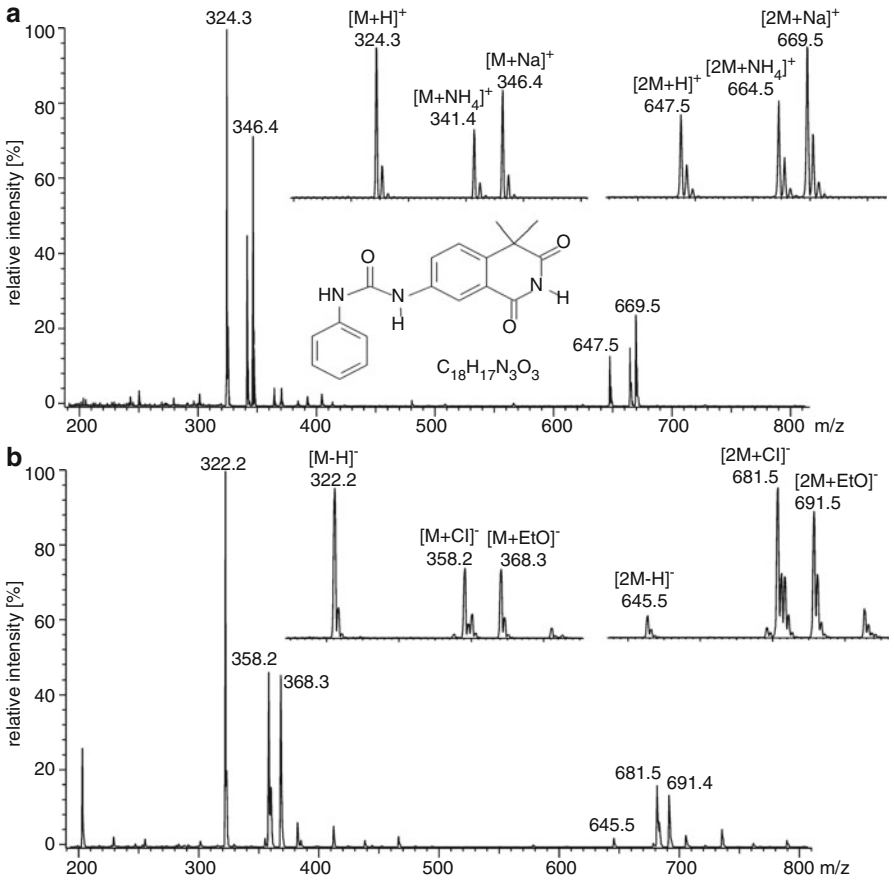

Fig. 12.31 Positive-ion (**a**) and negative-ion (**b**) nanoESI spectra of an anti-HIV drug from ethanol in the presence of ammonium chloride (By courtesy of H.-C. Kliem and M. Wiessler, German Cancer Research Center, Heidelberg)

12.6.2 ESI of Metal Complexes

In general, ESI can be well applied to ionic metal complexes and related compounds if these are soluble to at least 10^{-6} M in solvents suitable for the method [23–25]. Whether conventional or nanoESI should be employed basically depends on the tendency of the respective compounds towards decomposition. Labile complexes or compounds that are strongly adhesive to surfaces are preferably analyzed by nanoESI to avoid long-lasting contamination of the sample supply line. Illustrative examples in this field are presented by the application of ESI to isopoly metal oxyanions [150], polyphosphates [151], transition metal complexes (Fig. 12.32) [26, 152, 153], and cadmium sulfide clusters [154]. Furthermore, the

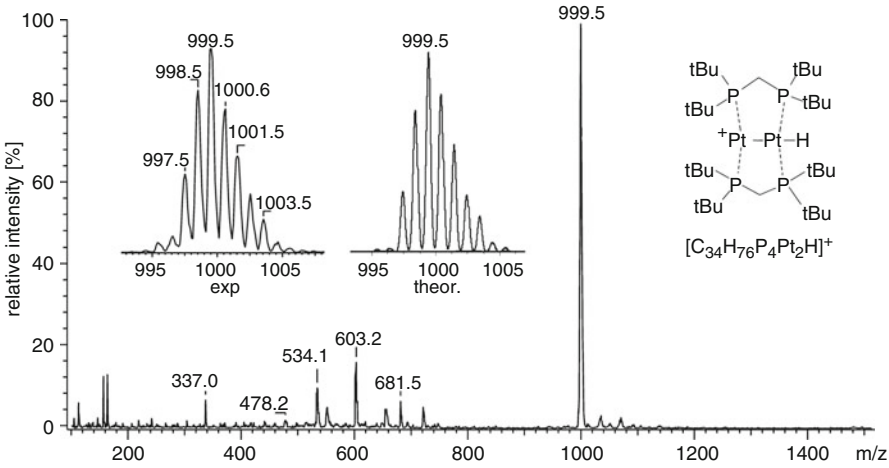

Fig. 12.32 Positive-ion ESI spectrum of a cationic dinuclear platinum hydride complex from dichloromethane solution. The *insets* compare experimental and theoretical isotopic patterns (By courtesy of P. Hofmann, Heidelberg University)

gas-phase reactions of electrosprayed metal complexes can be directly examined by tandem MS techniques (Sect. 9.17.1) [155–157].

12.6.3 ESI of Surfactants

Surfactants belong to a group of products where a low price is crucial, and therefore they are usually synthesized from coarsely defined mineral oil fractions or vegetable oils both of which represent (sometimes complex) mixtures (Fig. 12.33). Cationic and anionic surfactants are readily detected by ESI, but it also serves well for the detection of nonionic surfactants which tend to form $[M+alkali]^+$ or $[M–H]^-$ ions, respectively [158–162].

12.6.4 Oligonucleotides, DNA, and RNA

For the analysis of *oligonucleotides*, *DNA*, and *RNA* negative-ion ESI is best suited [145]. While MALDI becomes difficult beyond oligonucleotide 20-mers, ESI can handle much larger molecules [163–166]. The problems associated with mass spectrometry of oligonucleotides are due to the often multiple exchange of protons versus alkali ions (Sect. 11.5). Instead of ion exchange beads, nitrogen bases have proven very helpful in removing alkali ions from solutions [167]. In particular, the addition of 25 mM imidazole and piperidine yields very clean spectra (Fig. 12.34) [168]. Even after cation removal, these polyanionic species are demanding targets for MS.

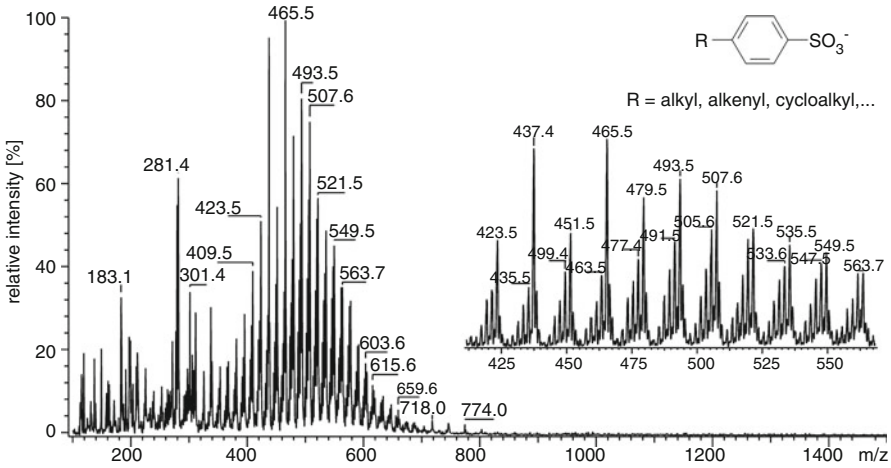

Fig. 12.33 Negative-ion ESI spectrum of an industrial cooling lubricant dissolved in 1-propanol at 1:1000. The dominant ions belong to alkylbenzene sulfonates. The *inset* expands the *m*/*z* 420–555 range, the most intensive peaks belonging to saturated alkyl chains (By courtesy of OMTEC GmbH, Eberbach)

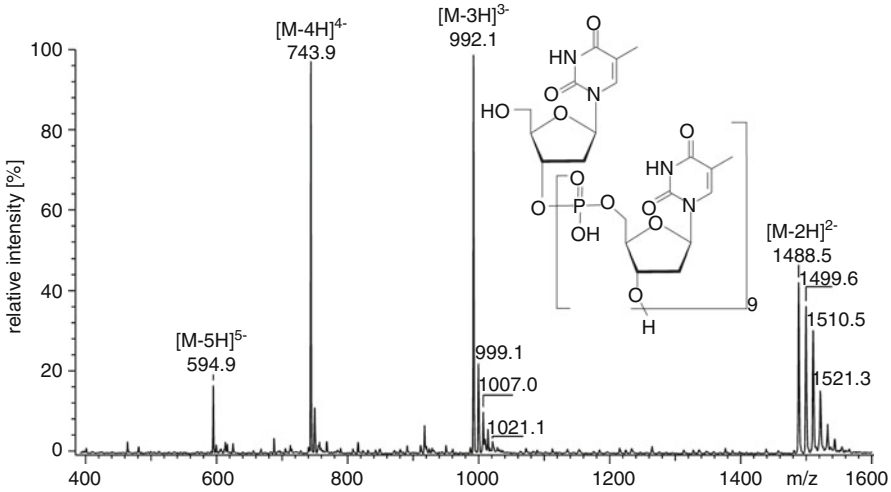

Fig. 12.34 Negative-ion ESI spectrum of the oligonucleotide dT_{10} in the presence of imidazole and piperidine. Here, H^+/Na^+ exchange is not completely suppressed (By courtesy of T. Krüger, University of Heidelberg)

Conventionally, oligonucleotides are presented by starting from the 5-hydroxyl terminus and writing along the phosphodiester chain towards the 3-hydroxyl terminus, i.e., from the 5′ to the 3′ end or from the phosphate to the ribose, respectively (Fig. 12.35). Oligonucleotides built from *nucleotides* based on the furanose ribose

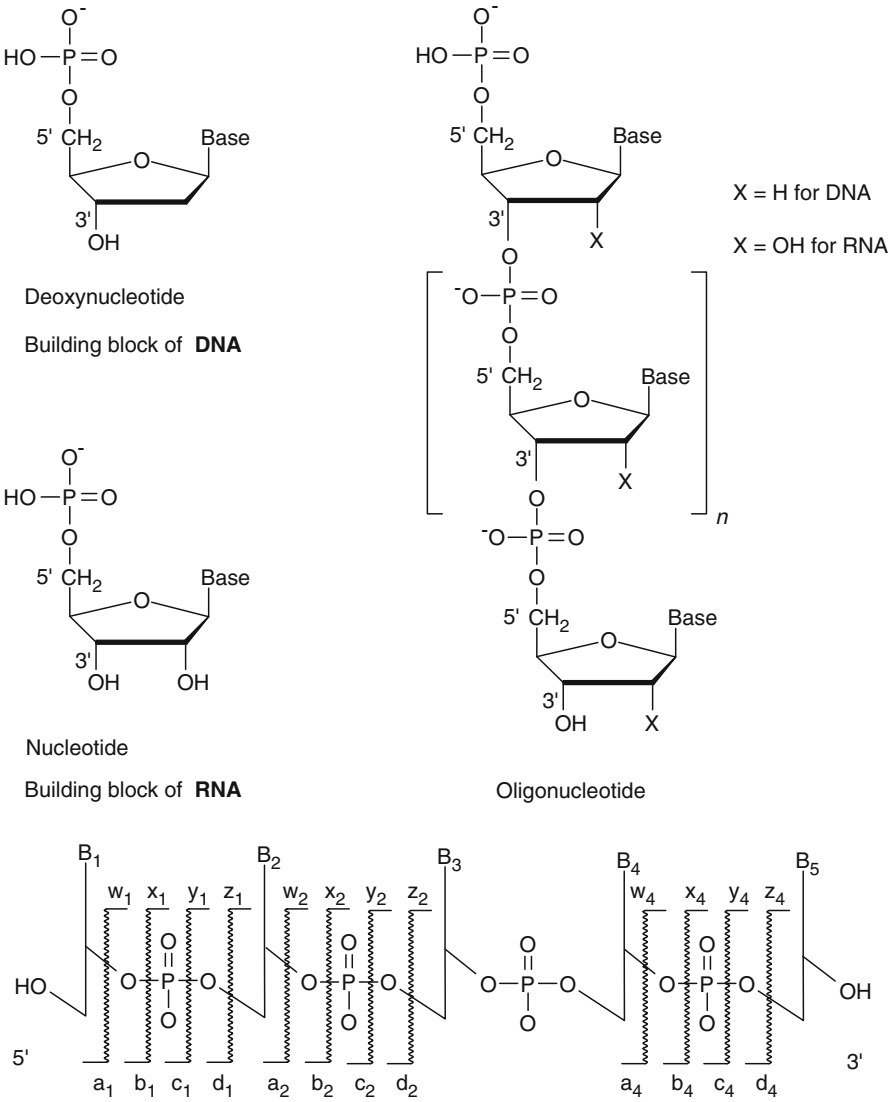

Fig. 12.35 Structures of nucleotides of DNA and RNA (*upper left*), general structure of oligonucleotides (*upper right*), and basic fragmentation scheme of oligonucleotides using the symbolized writing convention for the oligonucleotide backbone comprising furanose and *base* (*bottom*)

are termed *ribonucleic acids* (RNAs), those based on deoxyribose are termed *deoxyribonucleic acids* (DNAs). The bases attached to the pentose moieties are nitrogen-rich heterocyclic compounds.

Sequencing of oligonucleotides by ESI-MS/MS techniques is also feasible [163, 165, 169, 170]. Charged fragments of the 5′ end are denoted with letters and numerical subscripts from the beginning of the alphabet (*a*- to *d*-type ions) while fragments of the 3′ end are labeled as *w*- to *z*-type ions (Fig. 12.35) [171]. The bases on the ribose moieties are denoted either without qualification as base B_n with the subscripts starting on the 5′ end or by using the one-letter code of the entire nucleotides.

Sequence of an oligonucleotide The ESI-FT-ICR spectrum of $[M–4H]^{4–}$ ions of the phosphorothioate deoxyoligonucleotide 5′-GCCCAAGCTGGCATCCGTCA-3′ upon IRMPD exhibits numerous peaks corresponding to fragment ions of charge states from 1– to 4– (Fig. 12.36). This mass spectrum is greatly simplified upon charge deconvolution. Thanks to the resolving power of FT-ICR-MS, the assignment of charge states is absolutely reliable. In the resulting zero-charge spectrum, a_n-*B* and w_n fragment ions can be retrieved and the sequence thus derived [169].

12.6.5 ESI-MS of Oligosaccharides

Oligosaccharides [55, 74, 172, 173] as well as closely related compounds such as glycoproteins [73, 174], gangliosides [175], liposaccharides etc. are similar to oligonucleotides in that they require polar solvents and very soft ionization, in particular when the molecules are branched. As demonstrated by a large number of applications, ESI permits molecular weight determination and structure elucidation in these cases (Fig. 12.37; for a general fragmentation scheme cf. Sect. 11.5) [5].

12.6.6 Observing Supramolecular Chemistry at Work

The outstanding softness of ion formation of ESI allows to preserve noncovalent bonds during the sequence of ion liberation from solution into the gas phase. This can be observed by the formation of solvent adducts, cluster ions, and in particular, by its ability to deliver supramolecular systems into the gas phase [144, 176–180].

Formation of pseudorotaxanes The alkyl groups of secondary ammonium ions are able to barely pass through the cavity of benzo-21-crown-7 (**C7**) while phenyl groups require the wider cavity of dibenzo-24-crown-8 (**C8**) to form pseudorotaxanes. On the other side, phenyl groups suffice as stoppers to trap **C7** on the axle. The larger **C8** forms pseudorotaxanes even with secondary di*benzyl* ammonium ions. This can be directly observed by positive-ion ESI-MS of a mixture of suitably substituted ammonium ions as in case of a four-component self-sorting system consisting of **1**-H·PF6, **2**-H·PF6, **C7**, and **C8** (inset of Fig. 12.38) [178]. As anthracenyl and phenyl groups are present in **1**-H· PF6, it cannot overcome the barrier to insert into **C7**. Thus, only two peaks of high intensity are observed, i.e., for [**2**-H@**C7**]+, *m*/*z* 550, and for [**1**-H@**C8**]+, *m*/*z* 746. A weak peak indicating

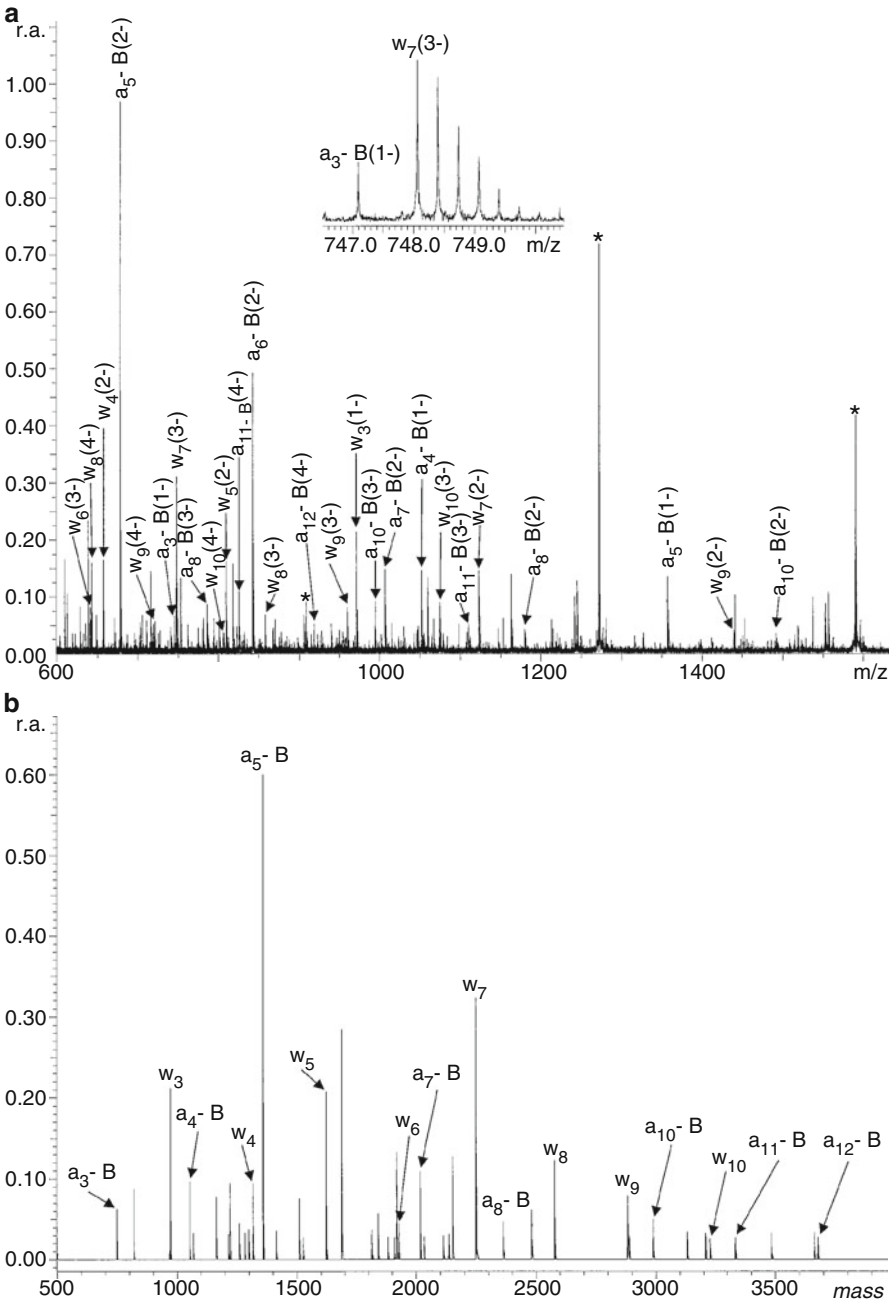

Fig. 12.36 ESI-FT-ICR IRMPD spectrum of negative ions of the phosphorothioate deoxyoligonucleotide 5′-GCCCAAGCTGGCATCCGTCA-3′. (**a**) The mass spectrum as obtained and (**b**) after charge deconvolution. Only the a_n-B and w_n fragment ions are labeled. In (**a**) peaks corresponding to residual precursor ions are labeled with an asterisk. The *inset* shows that closely spaced fragment ions can be resolved by FT-ICR-MS (Adapted from Ref. [169] with permission. © Elsevier, 2003)

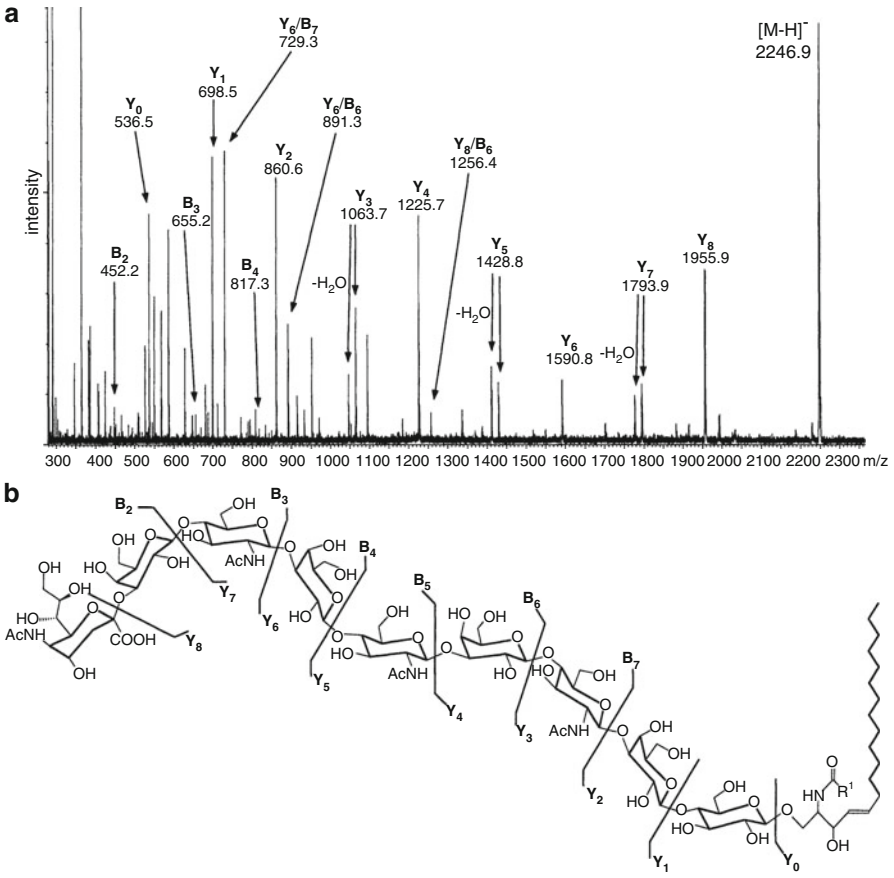

Fig. 12.37 (**a**) NanoESI-CID-MS/MS spectrum of the $[M–H]^-$ ion, *m/z* 2246.9, of a modified nonasaccharide obtained in a Q-TOF hybrid instrument and (**b**) proposed structure with fragments indicated (Reproduced from Ref. [175] by permission. © Elservier Science, 2001)

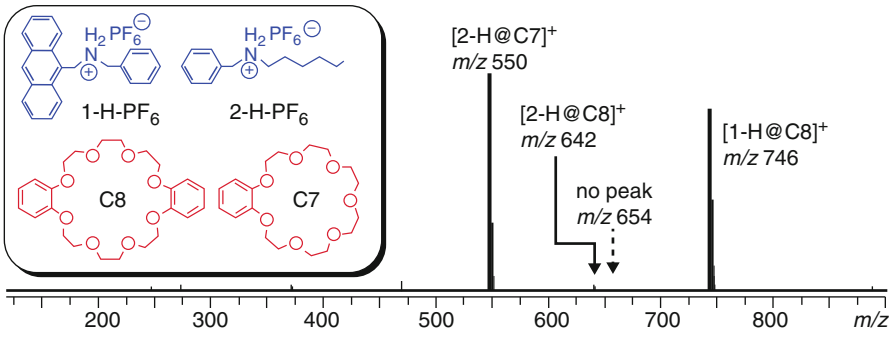

Fig. 12.38 Electrospray-ionization Fourier-transform ion-cyclotron-resonance (ESI-FT-ICR) mass spectrum of an equimolar mixture of **1**·H·PF6, **2**·H·PF6, **C7**, and **C8** in dichloromethane and their chemical structures (*inset*) (Reproduced from Ref. [178] with permission. © American Chemical Society, 2008)

[**2-**H@**C8**]+ is just visible at *m*/*z* 642. **1-**H+ and **C7,** in contrast, do not join into a complex as indicated by the missing peak at *m*/*z* 654.

12.6.7 High-Mass Proteins and Protein Complexes

The extraordinary high-mass capabilities of ESI allow for the analysis of proteins and protein complexes far beyond 10^6 u (>1 MDa) [14, 15, 21, 176, 177]. Even though the resulting ions are formed in very high charge states special mass analyzers with an expanded *m*/*z* range are required for this type of research.

Ions of 1 Mu The gram-negative spiral bacterium *Helicobacter pylori* is infecting almost half of the world's population. *H. pylori* possesses a very large multi-protein complex urease, which is essential for its survival in the acidic environment of the stomach. NanoESI has been used to establish the molecular weight of the 12-mer urease complex of 1,063,900 ± 600 u (Fig. 12.39) [15]. Spraying urease at higher

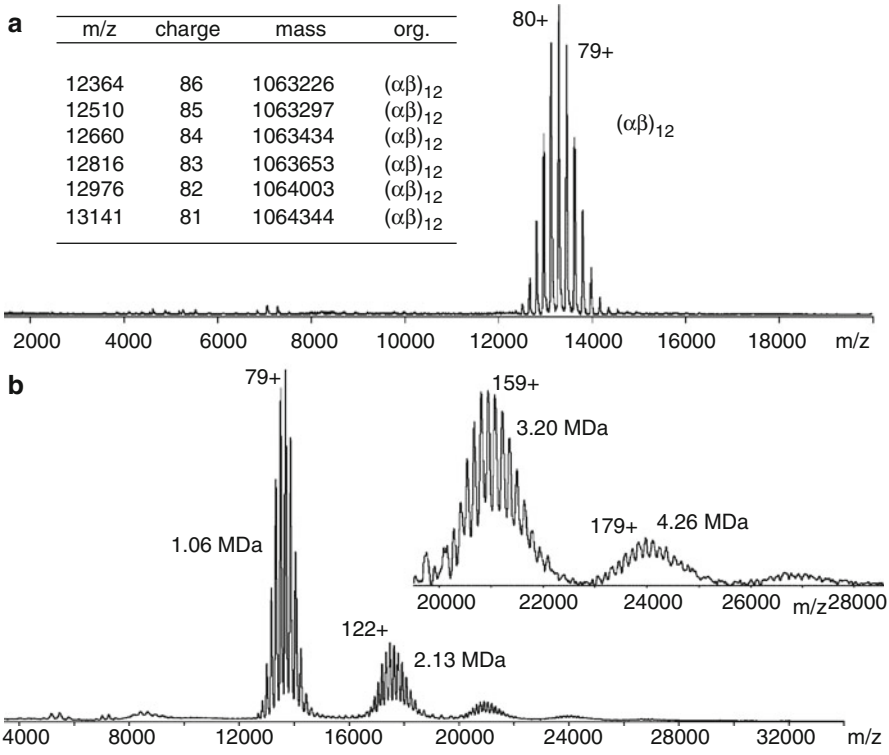

Fig. 12.39 NanoESI spectra of urease in 200 μM ammonium acetate at pH 8.0. (**a**) Using 20 μM urease mainly delivers $(\alpha\beta)_{12}$ subunits while (**b**) 40 μM concentration of the urease monomer also yield 24-, 36-, and even 48-mers (Adapted from Ref. [15] with permission. © Wiley Periodicals, Inc., 2004)

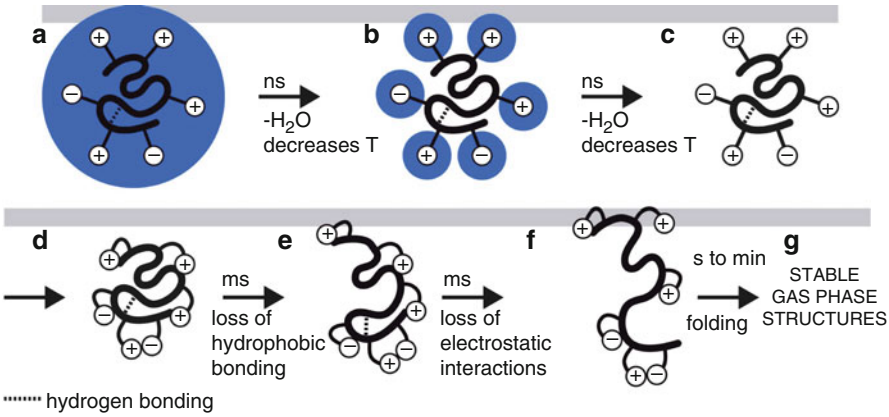

Fig. 12.40 Stepwise protein desolvation ($A \rightarrow C$), denaturization to an exterior-collapsed structure (D) and refolding to a stable gas-phase structure ($D \rightarrow G$) in transit from native solution phase to gas phase (Reproduced from Ref. [177] with permission. © The National Academy of Sciences of the USA, 2008)

concentration results in the formation of even larger protein complexes up to 48-mers of >4 Mu that are detected at up to about m/z 27,000 corresponding to charge states of >180+.

The question of whether or not proteins preserve their solution structure during ESI-MS has been addressed by Breuker and McLafferty [177]. According to their discussion, a protein ion loses the last hundred or so water molecules that are forming a monolayer around it during the very last steps of ion desolvation on the nanosecond timescale. The loss of water is accompanied by strong cooling of the protein ion, which finally collapses within several picoseconds as its exterior ionic interactions have been lost. Then, much slower during several milliseconds, the protein undergoes loss of hydrophobic bonding and of electrostatic interactions before it stabilizes over seconds to a final gas-phase conformation that is different from its native structure in solution. Due to the limited life time of the ions in normal ESI operation only the steps down to the cold exterior-collapsed structure can take place (Fig. 12.40).

12.7 Electrospray Roundup

Mode of Operation

In electrospray ionization an electrolytic solution is dissipated at atmospheric pressure by means of an electrostatic field to form an electrically charged aerosol. Aerosol formation is normally supported by a nebulizer gas (pneumatically-assisted ESI). Ions present in the charged droplets are liberated into the gas phase along a sequence of repeated droplet shrinking and droplet disintegration. During these steps, the mixture comprising gas, ions, and residual microdroplets is continuously transferred from the open atmosphere into the vacuum of the mass analyzer by

Table 12.1 Ions formed by ESI

Analytes	Positive ions	Negative ions
Low polarity	$[M+H]^+$, $[M+cat]^+$ if any at all[a]	$[M-H]^-$, $[M+an]^-$ if any at all[a]
Medium polarity	$[M+H]^+$, $[M+cat]^+$, $[M+alkali]^{+a}$	$[M-H]^-$, $[M+an]^{-a}$
Medium to high polarity	$[M+H]^+$, $[M+cat]^+$, $[M+alkali]^{+a}$ *exchange* $[M-H_n+alkali_{n+1}]^+$ {*clusters* $[2M+H]^+$, $[2M+alkali]^+$, *adducts* $[M+solv+H]^+$, $[M+solv+alkali]^+$}[c]	$[M-H]^-$, $[M+an]^{-a}$ *exchange* $[M-H_n+alkali_{n-1}]^-$ {*clusters* $[2M-H]^-$ *adducts* $[M+solv-H]^-$}[c]
Ionic[b]	C^+, $[C_n+A_{n-1}]^+$	A^-, $[C_{n-1}+A_n]^-$

[a]Some cation cat^+ or anion an^- incidentally present
[b]Comprising analyte cation C^+ and analyte anion A^-
[c]Braces denote less abundant species

means of an interface employing differential pumping stages. ESI is extremely soft as there is no ionization process involved that could impart energy on analyte molecules.

Analytes Suitable for Electrospray

As a general rule, ESI-MS can successfully be applied when the analyte is intrinsically ionic or can easily be transformed in solution phase to become ionic by protonation, deprotonation, cation attachment, or anion attachment. Thus, ESI can handle medium polar to ionic analytes from as low as 10 u to as high as 10^6 u in mass. ESI can deal equally well with ions of both polarities, whereas neutral nonpolar analytes are not suitable (Table 12.1).

The solvent may vary from volatile, nonpolar, and aprotic to moderately volatile, highly polar, and protic, e.g., diethylether, tetrahydrofuran, dichloromethane, trichloromethane, isopropanol, methanol, acetonitrile, water, and mixtures of these. Up to about 10% of dimethylsulfoxide or dimethylformamide can be tolerated in aqueous or methanolic solution. The addition of volatile acids or bases to promote ion formation is frequently employed. Volatile buffers and low concentrations of alkali ions ($<10^{-3}$ M) to promote cationization can be tolerated.

As a rule of thumb, less volatile solvents call for more sheath (nebulizer) gas (typical range is 1–3 l min^{-1}) and higher temperature of the desolvation gas or heated capillary (typical range is 150–250 °C), respectively. Both, insufficient desolvation and too strong desolvation will cause the ion formation to cease.

Types of Ions in ESI

Very similar to the previously introduced desorption methods ESI produces a variety of ions depending on the polarity of the analyte, the characteristics of the solvent, and on the presence or absence of impurities such as alkali metal or ammonium ions, for example. Radical ions are normally not observed (Table 12.1).

Sample Consumption

Sample consumption is chiefly determined by the concentration of the analyte solution and the liquid flow. For example, during a 1-min measurement conventional ESI consumes 4 pmol of sample when a 10^{-6} M solution is delivered at a flow of 4 µl min^{-1}. For nanoESI this reduces to 40 fmol for the same solution at 40 nl min^{-1}. Modern instruments have notably lower sample consumption, because recent interfaces transmit a much larger fraction of ions into the mass analyzer. Thus, while being operated at the same flow, very short acquisition times result in low volumes of sample solution.

Mass Analyzers for ESI

ESI and all other API sources are available in combination with all types of mass analyzers, i.e., basically one can choose any mass analyzer according to the analytical requirements. As fragment ions in ESI are often absent or at least exhibit very low abundance, analyzers capable of tandem MS and/or accurate mass measurement are preferred to provide an additional source of mass spectral information.

Comparison of ESI to APCI and APPI

The importance of ESI for LC-MS can be inferred from its wide range of analyte acceptance in terms of both polarity and mass. A graphical representation of the molecular weight and analyte polarity ranges covered by ESI, APCI, and APPI is best suited to give and impression of the preferred fields of application for these methods (Fig. 12.41). APCI and APPI, on the other hand, are very similar in coverage as both are accessing the lower left segment of the polarity-mass plane

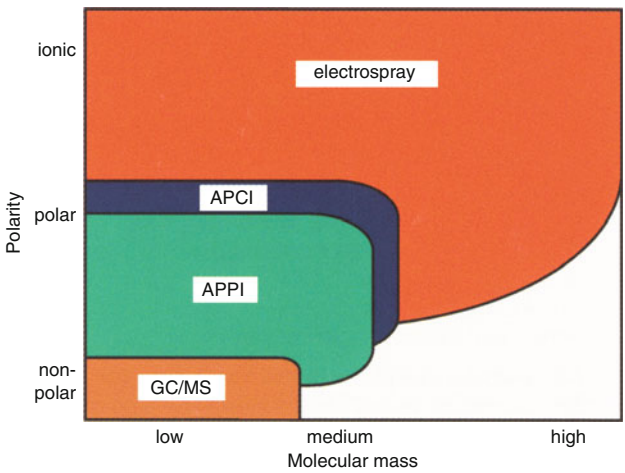

Fig. 12.41 ESI features a wide range of analyte acceptance in terms of both polarity and mass to handle medium polar to ionic analytes while APCI and APPI give access to the lower left segment of the polarity-mass plane (Adapted with permission of U. Karst from cover illustration of *Anal Bioanal Chem* 378(4), 2004. © Springer, Heidelberg, 2004)

in this illustration. APCI and APPI were discussed in the context of chemical ionization in Sects. 7.8 and 7.9.

References

1. Rossi DT, Sinz MW (eds) (2002) Mass Spectrometry in Drug Discovery. Marcel Dekker, New York
2. Schalley CA (ed) (2003) Modern Mass Spectrometry. Springer, New York
3. Ardrey RE (2003) Liquid Chromatography-Mass Spectrometry – An Introduction. Wiley, Chichester
4. Siuzdak G (2006) The Expanding Role of Mass Spectrometry in Biotechnology. MCC Press, San Diego
5. Lehmann WD (1996) Massenspektrometrie in der Biochemie. Spektrum Akademischer Verlag, Heidelberg
6. Dole RB (ed) (1997) Electrospray Ionization Mass Spectrometry – Fundamentals, Instrumentation and Applications. Wiley, Chichester. doi:10.17226/5702
7. Roboz J (1999) Mass Spectrometry in Cancer Research. CRC Press, Boca Raton. doi:10.1089/apc.1999.13.57
8. Chapman JR (ed) (2000) Mass Spectrometry of Proteins and Peptides. Humana Press, Totowa
9. Pramanik BN, Ganguly AK, Gross ML (eds) (2002) Applied Electrospray Mass Spectrometry. Marcel Dekker, New York
10. Cole RB (ed) (2010) Electrospray and MALDI Mass Spectrometry: Fundamentals, Instrumentation, Practicalities, and Biological Applications. Wiley, Hoboken
11. Lehmann WD (2010) Protein Phosphorylation Analysis by Electrospray Mass Spectrometry: A Guide to Concepts and Practice. Royal Society of Chemistry, Cambridge. doi:10.1007/s00265-010-1026-9
12. Amad MH, Cech NB, Jackson GS, Enke CG (2000) Importance of Gas-Phase Proton Affinities in Determining the Electrospray Ionization Response for Analytes and Solvents. J Mass Spectrom 35:784–789. doi:10.1002/1096-9888(200007)35:7<784::AID-JMS17>3.0.CO;2-Q
13. Schalley CA (2000) Supramolecular Chemistry Goes Gas Phase: The Mass Spectrometric Examination of Noncovalent Interactions in Host-Guest Chemistry and Molecular Recognition. Int J Mass Spectrom 194:11–39. doi:10.1016/S1387-3806(99)00243-2
14. Cristoni S, Bernardi LR (2003) Development of New Methodologies for the Mass Spectrometry Study of Bioorganic Macromolecules. Mass Spectrom Rev 22:369–406. doi:10.1002/mas.10062
15. Heck AJR, van den Heuvel RHH (2004) Investigation of Intact Protein Complexes by Mass Spectrometry. Mass Spectrom Rev 23:368–389. doi:10.1002/mas.10081
16. Fenn JB, Mann M, Meng CK, Wong SF, Whithouse CM (1989) Electrospray Ionization for Mass Spectrometry of Large Biomolecules. Science 246:64–71. doi:10.1126/science.2675315
17. Fenn JB, Mann M, Meng CK, Wong SF (1990) Electrospray Ionization – Principles and Practice. Mass Spectrom Rev 9:37–70. doi:10.1002/mas.1280090103
18. Smith RD, Loo JA, Edmonds CG, Barinaga CJ, Udseth HR (1990) New Developments in Biochemical Mass Spectrometry: Electrospray Ionization. Anal Chem 62:882–899. doi:10.1021/ac00208a002
19. Fenn JB (2003) Electrospray: Wings for Molecular Elephants (Nobel Lecture). Angew Chem, Int Ed 42:3871–3894. doi:10.1002/anie.200300605
20. Fuerstenau SD, Benner WH (1995) Molecular Weight Determination of Megadalton DNA Electrospray Ions Using Charge Detection Time-of-Flight Mass Spectrometry. Rapid Commun Mass Spectrom 9:1528–1538. doi:10.1002/rcm.1290091513

21. Fuerstenau SD, Benner WH, Thomas JJ, Brugidou C, Bothner B, Suizdak G (2001) Mass Spectrometry of an Intact Virus. Angew Chem Int Ed 40:541–544. doi:10.1002/1521-3773(20010202)40:3<541::AID-ANIE541>3.0.CO;2-K
22. Felitsyn N, Peschke M, Kebarle P (2002) Origin and Number of Charges Observed on Multiply-Protonated Native Proteins Produced by ESI. Int J Mass Spectrom 219:39–62. doi:10.1016/S1387-3806(02)00588-2
23. Colton R, D'Agostino A, Traeger JC (1995) Electrospray Mass Spectrometry Applied to Inorganic and Organometallic Chemistry. Mass Spectrom Rev 14:79–106. doi:10.1002/mas.1280140203
24. Traeger JC (2000) Electrospray Mass Spectrometry of Organometallic Compounds. Int J Mass Spectrom 200:387–401. doi:10.1016/S1387-3806(00)00346-8
25. Henderson W, McIndoe SJ (2005) Mass Spectrometry of Inorganic and Organometallic Compounds. Wiley, Chichester. doi:10.1002/cfg.467
26. Poon GK, Bisset GMF, Mistry P (1993) Electrospray Ionization Mass Spectrometry for Analysis of Low-Molecular-Weight Anticancer Drugs and Their Analogs. J Am Soc Mass Spectrom 4:588–595. doi:10.1016/1044-0305(93)85020-X
27. Winger BE, Light-Wahl KJ, Ogorzalek Loo RR, Udseth HR, Smith RD (1993) Observation and Implications of High Mass-to-Charge Ratio Ions from Electrospray Ionization Mass Spectrometry. J Am Soc Mass Spectrom 4:536–545. doi:10.1016/1044-0305(93)85015-P
28. Wang Y, Schubert M, Ingendoh A, Franzen J (2000) Analysis of Non-Covalent Protein Complexes Up to 290 kDa Using Electrospray Ionization and Ion Trap Mass Spectrometry. Rapid Commun Mass Spectrom 14:12–17. doi:10.1002/(SICI)1097-0231(20000115)14:1<12::AID-RCM825>3.0.CO;2-7
29. Sobott F, Hernández H, McCammon MG, Tito MA, Robinson CV (2002) A Tandem Mass Spectrometer for Improved Transmission and Analysis of Large Macromolecular Assemblies. Anal Chem 74:1402–1407. doi:10.1021/ac0110552
30. Covey TR, Thomson BA, Schneider BB (2009) Atmospheric Pressure Ion Sources. Mass Spectrom Rev 28:870–897. doi:10.1002/mas.20246
31. Horning EC, Horning MG, Carroll DI, Dzidic I, Stillwell RN (1973) New Picogram Detection System Based on a Mass Spectrometer with an External Ionization Source at Atmospheric Pressure. Anal Chem 45:936–943. doi:10.1021/ac60328a035
32. Horning EC, Carroll DI, Dzidic I, Haegele KD, Horning MG, Stillwell RN (1974) Atmospheric Pressure Ionization (API) Mass Spectrometry. Solvent-Mediated Ionization of Samples Introduced in Solution and in a Liquid Chromatograph Effluent Stream. J Chromatogr Sci 12:725–729. doi:10.1093/chromsci/12.11.725
33. Robb DB, Covey TR, Bruins AP (2000) Atmospheric Pressure Photoionization: an Ionization Method for Liquid Chromatography-Mass Spectrometry. Anal Chem 72:3653–3659. doi:10.1021/ac0001636
34. Blakley CR, Carmody JJ, Vestal ML (1980) A New Soft Ionization Technique for Mass Spectrometry of Complex Molecules. J Am Chem Soc 102:5931–5933. doi:10.1021/ja00538a050
35. Blakley CR, Vestal ML (1983) Thermospray Interface for Liquid Chromatography/Mass Spectrometry. Anal Chem 55:750–754. doi:10.1021/ac00255a036
36. Vestal ML (1983) Studies of Ionization Mechanisms Involved in Thermospray LC-MS. Int J Mass Spectrom Ion Phys 46:193–196. doi:10.1016/0020-7381(83)80086-2
37. Wilkes JG, Freeman JP, Heinze TM, Lay JO Jr, Vestal ML (1995) AC Corona-Discharge Aerosol-Neutralization Device Adapted to Liquid Chromatography/Particle Beam/Mass Spectrometry. Rapid Commun Mass Spectrom 9:138–142. doi:10.1002/rcm.1290090207
38. Vestal ML (1984) High-Performance Liquid Chromatography-Mass Spectrometry. Science 226:275–281. doi:10.1126/science.6385251
39. Evans CA Jr, Hendricks CD (1972) Electrohydrodynamic Ion Source for the Mass Spectrometry of Liquids. Rev Sci Inst 43:1527–1530. doi:10.1063/1.1685481

40. Simons DS, Colby BN, Evans CA Jr (1974) Electrohydrodynamic Ionization Mass Spectrometry. Ionization of Liquid Glycerol and Nonvolatile Organic Solutes. Int J Mass Spectrom Ion Phys 15:291–302. doi:10.1016/0020-7381(74)85006-0
41. Zeleny J (1917) Instability of Electrified Liquid Surfaces. Phys Rev 10:1–7. doi:10.1103/PhysRev.10.1
42. Taylor GI (1964) Disintegration of Water Drops in an Electric Field. Proc Royal Soc London A 280:383–397. doi:10.1098/rspa.1964.0151
43. Rayleigh L (1882) On the Equilibrium of Liquid Conducting Masses Charged with Electricity. Dublin Phil Mag J Sci (London/Edinburgh) 14:184–186. doi:10.1080/14786448208628425
44. Dülcks T, Röllgen FW (1995) Ionization Conditions and Ion Formation in Electrohydrodynamic Mass Spectrometry. Int J Mass Spectrom Ion Proc 148:123–144. doi:10.1016/0168-1176(95)04250-O
45. Dülcks T, Röllgen FW (1995) Ion Source for Electrohydrodynamic Mass Spectrometry. J Mass Spectrom 30:324–332. doi:10.1002/jms.1190300215
46. Cook KD (1986) Electrohydrodynamic Mass Spectrometry. Mass Spectrom Rev 5:467–519. doi:10.1002/mas.1280050404
47. Dole M, Mack LL, Hines RL, Mobley RC, Ferguson LD, Alice MB (1968) Molecular Beams of Macroions. J Chem Phys 49:2240–2249. doi:10.1063/1.1670391
48. Dole M, Hines RL, Mack LL, Mobley RC, Ferguson LD, Alice MB (1968) Gas Phase Macroions. Macromolecules 1:96–97. doi:10.1021/ma60001a017
49. Gieniec J, Mack LL, Nakamae K, Gupta C, Kumar V, Dole M (1984) Electrospray Mass Spectroscopy of Macromolecules: Application of an Ion-Drift Spectrometer. Biomed Mass Spectrom 11:259–268. doi:10.1002/bms.1200110602
50. Yamashita M, Fenn JB (1984) Electrospray Ion Source. Another Variation on the Free-Jet Theme. J Phys Chem 88:4451–4459. doi:10.1021/j150664a002
51. Yamashita M, Fenn JB (1984) Negative Ion Production with the Electrospray Ion Source. J Phys Chem 88:4671–4675. doi:10.1021/j150664a046
52. Whitehouse CM, Robert RN, Yamashita M, Fenn JB (1985) Electrospray Interface for Liquid Chromatographs and Mass Spectrometers. Anal Chem 57:675–679. doi:10.1021/ac00280a023
53. Bruins AP (1991) Mass Spectrometry with Ion Sources Operating at Atmospheric Pressure. Mass Spectrom Rev 10:53–77. doi:10.1002/mas.1280100104
54. Kebarle P, Tang L (1993) From Ions in Solution to Ions in the Gas Phase – The Mechanism of Electrospray Mass Spectrometry. Anal Chem 65:972A–986A. doi:10.1021/ac00070a001
55. Karas M, Bahr U, Dülcks T (2001) Nano-Electrospray Ionization Mass Spectrometry: Addressing Analytical Problems Beyond Routine. Fresenius J Anal Chem 366:669–676. doi:10.1007/s002160051561
56. Anacleto JF, Pleasance S, Boyd RK (1992) Calibration of Ion Spray Mass Spectra Using Cluster Ions. Org Mass Spectrom 27:660–666. doi:10.1002/oms.1210270603
57. Hop CECA (1996) Generation of High Molecular Weight Cluster Ions by Electrospray Ionization; Implications for Mass Calibration. J Mass Spectrom 31:1314–1316. doi:10.1002/(SICI)1096-9888(199611)31:11<1314::AID-JMS429>3.0.CO;2-N
58. Kantrowitz A, Grey J (1951) High Intensity Source for the Molecular Beam. I. Theoretical. Rev Sci Inst 22:328–332. doi:10.1063/1.1745921
59. Fenn JB (2000) Mass Spectrometric Implications of High-Pressure Ion Sources. Int J Mass Spectrom 200:459–478. doi:10.1016/S1387-3806(00)00328-6
60. Klee S, Derpmann V, Wissdorf W, Klopotowski S, Kersten H, Brockmann KJ, Benter T, Albrecht S, Bruins AP, Dousty F, Kauppila TJ, Kostiainen R, O'Brien R, Robb DB, Syage JA (2014) Are Clusters Important in Understanding the Mechanisms in Atmospheric Pressure Ionization? Part 1: Reagent Ion Generation and Chemical Control of Ion Populations. J Am Soc Mass Spectrom 25:1310–1321. doi:10.1007/s13361-014-0891-2

61. Bruins AP, Covey TR, Henion JD (1987) Ion Spray Interface for Combined Liquid Chromatography/Atmospheric Pressure Ionization Mass Spectrometry. Anal Chem 59:2642–2646. doi:10.1021/ac00149a003
62. Covey TR, Bruins AP, Henion JD (1988) Comparison of Thermospray and Ion Spray Mass Spectrometry in an Atmospheric Pressure Ion Source. Org Mass Spectrom 23:178–186. doi:10.1002/oms.1210230305
63. Covey TR, Bonner RF, Shushan BI, Henion JD (1988) The Determination of Protein, Oligonucleotide, and Peptide Molecular Weights by Ion-Spray Mass Spectrometry. Rapid Commun Mass Spectrom 2:249–256. doi:10.1002/rcm.1290021111
64. Ikonomou MG, Blades AT, Kebarle P (1991) Electrospray – Ion Spray: A Comparison of Mechanisms and Performance. Anal Chem 63:1989–1998. doi:10.1021/ac00018a017
65. Smith RD, Barinaga CJ, Udseth HR (1988) Improved Electrospray Ionization Interface for Capillary Zone Electrophoresis-Mass Spectrometry. Anal Chem 60:1948–1952. doi:10.1021/ac00169a022
66. Abian J (1999) The Coupling of Gas and Liquid Chromatography with Mass Spectrometry. J Mass Spectrom 34:157–168. doi:10.1002/(SICI)1096-9888(199903)34:3<157::AID-JMS804>3.0.CO;2-4
67. Shaffer SA, Tang K, Anderson GA, Prior DC, Udseth HR, Smith RD (1997) A Novel Ion Funnel for Focusing Ions at Elevated Pressure Using Electrospray Ionization Mass Spectrometry. Rapid Commun Mass Spectrom 11:1813–1817. doi:10.1002/(SICI)1097-0231(19971030)11:16<1813::AID-RCM87>3.0.CO;2-D
68. Shaffer SA, Prior DC, Anderson GA, Udseth HR, Smith RD (1998) An Ion Funnel Interface for Improved Ion Focusing and Sensitivity Using Electrospray Ionization Mass Spectrometry. Anal Chem 70:4111–4119. doi:10.1021/ac9802170
69. Kim T, Tolmachev AV, Harkewicz R, Prior DC, Anderson G, Udseth HR, Smith RD, Bailey TH, Rakov S, Futrell JH (2000) Design and Implementation of a New Electrodynamic Ion Funnel. Anal Chem 72:2247–2255. doi:10.1021/ac991412x
70. Ibrahim Y, Belov ME, Tolmachev AV, Prior DC, Smith RD (2007) Ion Funnel Trap Interface for Orthogonal Time-of-Flight Mass Spectrometry. Anal Chem 79:7845–7852. doi:10.1021/ac071091m
71. Ibrahim YM, Belov ME, Liyu AV, Smith RD (2008) Automated Gain Control Ion Funnel Trap for Orthogonal Time-of-Flight Mass Spectrometry. Anal Chem 80:5367–5376. doi:10.1021/ac8003488
72. Smith RD, Loo JA, Barinaga CJ, Edmonds CG, Udseth HR (1990) Collisional Activation and Collision-Activated Dissociation of Large Multiply Charged Polypeptides and Proteins Produced by Electrospray Ionization. J Am Soc Mass Spectrom 1:53–65. doi:10.1016/1044-0305(90)80006-9
73. Harvey DJ (2000) Collision-Induced Fragmentation of Underivatized *N*-Linked Carbohydrates Ionized by Electrospray. J Mass Spectrom 35:1178–1190. doi:10.1002/1096-9888(200010)35:10<1178::AID-JMS46>3.0.CO;2-F
74. Schmidt A, Bahr U, Karas M (2001) Influence of Pressure in the First Pumping Stage on Analyte Desolvation and Fragmentation in Nano-ESI MS. Anal Chem 71:6040–6046. doi:10.1021/ac010451h
75. Jedrzejewski PT, Lehmann WD (1997) Detection of Modified Peptides in Enzymatic Digests by Capillary Liquid Chromatography/Electrospray Mass Spectrometry and a Programmable Skimmer CID Acquisition Routine. Anal Chem 69:294–301. doi:10.1021/ac9606618
76. Weinmann W, Stoertzel M, Vogt S, Svoboda M, Schreiber A (2001) Tuning Compounds for Electrospray Ionization/in-Source Collision-Induced Dissociation and Mass Spectra Library Searching. J Mass Spectrom 36:1013–1023. doi:10.1002/jms.201
77. Huddleston MJ, Bean MF, Carr SA (1993) Collisional Fragmentation of Glycopeptides by Electrospray Ionization LC/MS and LC/MS/MS: Methods for Selective Detection of Glycopeptides in Protein Digests. Anal Chem 65:877–884. doi:10.1021/ac00055a009

78. Chen H, Tabei K, Siegel MM (2001) Biopolymer Sequencing Using a Triple Quadrupole Mass Spectrometer in the ESI Nozzle-Skimmer/Precursor Ion MS/MS Mode. J Am Soc Mass Spectrom 12:846–852. doi:10.1016/S1044-0305(01)00258-6
79. Hoogland FG, Boon JJ (2009) Development of MALDI-MS and Nano-ESI-MS Methodology for the Full Identification of Poly(ethylene glycol) Additives in Artists' Acrylic Paints. Int J Mass Spectrom 284:66–71. doi:10.1016/j.ijms.2009.03.002
80. Miao X-S, Metcalfe CD (2003) Determination of Carbamazepine and Its Metabolites in Aqueous Samples Using Liquid Chromatography-Electrospray Tandem Mass Spectrometry. Anal Chem 75:3731–3738. doi:10.1021/ac030082k
81. Gross JH, Eckert A, Siebert W (2002) Negative-Ion Electrospray Mass Spectra of Carbon Dioxide-Protected *N*-Heterocyclic Anions. J Mass Spectrom 37:541–543. doi:10.1002/jms.302
82. Wilm MS, Mann M (1994) Electrospray and Taylor-Cone Theory, Dole's Beam of Macromolecules at Last? Int J Mass Spectrom Ion Proc 136:167–180. doi:10.1016/0168-1176(94)04024-9
83. Wilm M, Mann M (1996) Analytical Properties of the Nanoelectrospray Ion Source. Anal Chem 68:1–8. doi:10.1021/ac9509519
84. Wilm M, Shevshenko A, Houthaeve T, Breit S, Schweigerer L, Fotsis T, Mann M (1996) Femtomole Sequencing of Proteins from Polyacrylamide Gels by Nano-Electrospray Mass Spectrometry. Nature 379:466–469. doi:10.1038/379466a0
85. Juraschek R, Dülcks T, Karas M (1999) Nanoelectrospray – More Than Just a Minimized-Flow Electrospray Ionization Source. J Am Soc Mass Spectrom 10:300–308. doi:10.1016/S1044-0305(98)00157-3
86. Guo M, Huang BX, Kim HY (2009) Conformational Changes in Akt1 Activation Probed by Amide Hydrogen/Deuterium Exchange and Nano-Electrospray Ionization Mass Spectrometry. Rapid Commun Mass Spectrom 23:1885–1891. doi:10.1002/rcm.4085
87. Gibson GTT, Mugo SM, Oleschuk RD (2009) Nanoelectrospray Emitters: Trends and Perspective. Mass Spectrom Rev 28:918–936. doi:10.1002/mas.20248
88. Valaskovic GA, Murphy JP, Lee MS (2004) Automated Orthogonal Control System for Electrospray Ionization. J Am Soc Mass Spectrom 15:1201–1215. doi:10.1016/j.jasms.2004.04.033
89. Kebarle P, Verkerk UH (2009) Electrospray: From Ions in Solution to Ions in the Gas Phase, What We Know Now. Mass Spectrom Rev 28:898–917. doi:10.1002/mas.20247
90. Cole RB (2000) Some Tenets Pertaining to Electrospray Ionization Mass Spectrometry. J Mass Spectrom 35:763–772. doi:10.1002/1096-9888(200007)35:7<763::AID-JMS16>3.0.CO;2-%23
91. Kebarle P (2000) A Brief Overview of the Present Status of the Mechanisms Involved in Electrospray Mass Spectrometry. J Mass Spectrom 35:804–817. doi:10.1002/1096-9888(200007)35:7<804::AID-JMS22>3.0.CO;2-Q
92. Marginean I, Nemes P, Parvin L, Vertes A (2006) How Much Charge Is There on a Pulsating Taylor Cone? Appl Phys Lett 89:064104-1-064104/3. doi:10.1063/1.2266889
93. Nemes P, Marginean I, Vertes A (2007) Spraying Mode Effect on Droplet Formation and Ion Chemistry in Electrosprays. Anal Chem 79:3105–3116. doi:10.1021/ac062382i
94. de la Mora JF, Van Berkel GJ, Enke CG, Cole RB, Martinez-Sanchez M, Fenn JB (2000) Electrochemical Processes in Electrospray Ionization Mass Spectrometry. J Mass Spectrom 35:939–952. doi:10.1002/1096-9888(200008)35:8<939::AID-JMS36>3.0.CO;2-V
95. Van Berkel GJ (2000) Electrolytic Deposition of Metals on to the High-Voltage Contact in an Electrospray Emitter: Implications for Gas-Phase Ion Formation. J Mass Spectrom 35:773–783. doi:10.1002/1096-9888(200007)35:7<773::AID-JMS4>3.0.CO;2-6
96. Schäfer M, Drayue M, Springer A, Zacharias P, Meerholz K (2007) Radical Cations in Electrospray Mass Spectrometry: Formation of Open-Shell Species, Examination of the Fragmentation Behavior in ESI-MS^n and Reaction Mechanism Studies by Detection of Transient Radical Cations. Eur J Org Chem 2007:5162–5174. doi:10.1002/ejoc.200700199

97. Gomez A, Tang K (1994) Charge and Fission of Droplets in Electrostatic Sprays. Phys Fluids 6:404–414. doi:10.1063/1.868037
98. Duft D, Achtzehn T, Müller R, Huber BA, Leisner T (2003) Coulomb Fission. Rayleigh Jets from Levitated Microdroplets. Nature 421:128. doi:10.1038/421128a
99. Grimm RL, Beauchamp JL (2005) Dynamics of Field-Induced Droplet Ionization: Time-Resolved Studies of Distortion, Jetting, and Progeny Formation from Charged and Neutral Methanol Droplets Exposed to Strong Electric Fields. J Phys Chem B 109:8244–8250. doi:10.1021/jp0450540
100. Mack LL, Kralik P, Rheude A, Dole M (1970) Molecular Beams of Macroions, II. J Chem Phys 52:4977–4986. doi:10.1063/1.1672733
101. Iribarne JV, Thomson BA (1976) On the Evaporation of Small Ions from Charged Droplets. J Chem Phys 64:2287–2294. doi:10.1063/1.432536
102. Thomson BA, Iribarne JV (1979) Field-Induced Ion Evaporation from Liquid Surfaces at Atmospheric Pressure. J Chem Phys 71:4451–4463. doi:10.1063/1.438198
103. Labowsky M, Fenn JB, de la Mora JF (2000) A Continuum Model for Ion Evaporation from a Drop: Effect of Curvature and Charge on Ion Solvation Energy. Anal Chim Acta 406:105–118. doi:10.1016/S0003-2670(99)00595-4
104. Fenn JB (1993) Ion Formation from Charged Droplets: Roles of Geometry, Energy, and Time. J Am Soc Mass Spectrom 4:524–535. doi:10.1016/1044-0305(93)85014-O
105. Fenn JB, Rosell J, Meng CK (1997) In Electrospray Ionization, How Much Pull Does an Ion Need to Escape Its Droplet Prison? J Am Soc Mass Spectrom 8:1147–1157. doi:10.1016/S1044-0305(97)00161-X
106. Loo JA, Edmonds CG, Udseth HR, Smith RD (1990) Effect of Reducing Disulfide-Containing Proteins on Electrospray Ionization Mass Spectra. Anal Chem 62:693–698. doi:10.1021/ac00206a009
107. Chowdhury SK, Katta V, Chait BT (1990) Probing Conformational Changes in Proteins by Mass Spectrometry. J Am Chem Soc 112:9012–9013. doi:10.1021/ja00180a074
108. Nemes P, Goyal S, Vertes A (2008) Conformational and Noncovalent Complexation Changes in Proteins During Electrospray Ionization. Anal Chem 80:387–395. doi:10.1021/ac0714359
109. Schmelzeisen-Redeker G, Bütfering L, Röllgen FW (1989) Desolvation of Ions and Molecules in Thermospray Mass Spectrometry. Int J Mass Spectrom Ion Proc 90:139–150. doi:10.1016/0168-1176(89)85004-9
110. Williams ER (1996) Proton Transfer Reactivity of Large Multiply Charged Ions. J Mass Spectrom 31:831–842. doi:10.1002/(SICI)1096-9888(199608)31:8<831::AID-JMS392>3.0.CO;2-7
111. Iavarone AT, Jurchen JC, Williams ER (2001) Supercharged Protein and Peptide Ions Formed by Electrospray Ionization. Anal Chem 73:1455–1460. doi:10.1021/ac001251t
112. Iavarone AT, Williams ER (2002) Supercharging in Electrospray Ionization: Effects on Signal and Charge. Int J Mass Spectrom 219:63–72. doi:10.1016/S1387-3806(02)00587-0
113. Iavarone AT, Williams ER (2003) Mechanism of Charging and Supercharging Molecules in Electrospray Ionization. J Am Chem Soc 125:2319–2327. doi:10.1021/ja021202t
114. Youhnovski N, Matecko I, Samalikova M, Grandori R (2005) Characterization of Cytochrome c Unfolding by Nano-Electrospray Ionization Time-of-Flight and Fourier Transform Ion Cyclotron Resonance Mass Spectrometry. Eur J Mass Spectrom 11:519–524. doi:10.1255/ejms.730
115. Dobo A, Kaltashov IA (2001) Detection of Multiple Protein Conformational Ensembles in Solution Via Deconvolution of Charge-State Distributions in ESI-MS. Anal Chem 73:4763–4773. doi:10.1021/ac010713f
116. Chapman JR, Gallagher RT, Barton EC, Curtis JM, Derrick PJ (1992) Advantages of High-Resolution and High-Mass Range Magnetic-Sector Mass Spectrometry for Electrospray Ionization. Org Mass Spectrom 27:195–203. doi:10.1002/oms.1210270308
117. Cole RB, Harrata AK (1993) Solvent Effect on Analyte Charge State, Signal Intensity, and Stability in Negative Ion Electrospray Mass Spectrometry – Implications for the Mechanism of Negative Ion Formation. J Am Soc Mass Spectrom 4:546–556. doi:10.1016/1044-0305(93)85016-Q

118. Straub RF, Voyksner RD (1993) Negative Ion Formation in Electrospray Mass Spectrometry. J Am Soc Mass Spectrom 4:578–587. doi:10.1016/1044-0305(93)85019-T
119. Saf R, Mirtl C, Hummel K (1994) Electrospray Mass Spectrometry Using Potassium Iodide in Aprotic Organic Solvents for the Ion Formation by Cation Attachment. Tetrahedron Lett 35:6653–6656. doi:10.1016/S0040-4039(00)73459-9
120. Cody RB, Tamura J, Musselman BD (1992) Electrospray Ionization/Magnetic Sector Mass Spectrometry: Calibration, Resolution, and Accurate Mass Measurements. Anal Chem 64:1561–1570. doi:10.1021/ac00038a012
121. Mann M, Meng CK, Fenn JB (1989) Interpreting Mass Spectra of Multiply Charged Ions. Anal Chem 61:1702–1708. doi:10.1021/ac00190a023
122. Labowsky M, Whitehouse CM, Fenn JB (1993) Three-Dimensional Deconvolution of Multiply Charged Spectra. Rapid Commun Mass Spectrom 7:71–84. doi:10.1002/rcm.1290070117
123. Zhang Z, Marshall AG (1998) A Universal Algorithm for Fast and Automated Charge State Deconvolution of Electrospray Mass-to-Charge Ratio Spectra. J Am Soc Mass Spectrom 9:225–233. doi:10.1016/S1044-0305(97)00284-5
124. Maleknia SD, Downard KM (2005) Charge Ratio Analysis Method to Interpret High Resolution Electrospray Fourier Transform-Ion Cyclotron Resonance Mass Spectra. Int J Mass Spectrom 246:1–9. doi:10.1016/j.ijms.2005.08.002
125. Maleknia SD, Downard KM (2005) Charge Ratio Analysis Method: Approach for the Deconvolution of Electrospray Mass Spectra. Anal Chem 77:111–119. doi:10.1021/ac048961+
126. Lu W, Callahan JH, Fry FS, Andrzejewski D, Musser SM, Harrington PD (2011) A Discriminant Based Charge Deconvolution Analysis Pipeline for Protein Profiling of Whole Cell Extracts Using Liquid Chromatography-Electrospray Ionization-Quadrupole Time-of-Flight Mass Spectrometry. Talanta 84:1180–1187. doi:10.1016/j.talanta.2011.03.024
127. Maleknia SD, Green DC (2010) ECRAM Computer Algorithm for Implementation of the Charge Ratio Analysis Method to Deconvolute Electrospray Ionization Mass Spectra. Int J Mass Spectrom 290:1–8. doi:10.1016/j.ijms.2009.10.005
128. Winkler R (2010) ESIprot: a Universal Tool for Charge State Determination and Molecular Weight Calculation of Proteins from Electrospray Ionization Mass Spectrometry Data. Rapid Commun Mass Spectrom 24:285–294. doi:10.1002/rcm.4384
129. Wada Y (2016) Mass Spectrometry of Transferrin and Apolipoprotein C-III for Diagnosis and Screening of Congenital Disorder of Glycosylation. Glycoconjug J 33:297–307. doi:10.1007/s10719-015-9636-0
130. Dobberstein P, Schroeder E (1993) Accurate Mass Determination of a High Molecular Weight Protein Using Electrospray Ionization with a Magnetic Sector Instrument. Rapid Commun Mass Spectrom 7:861–864. doi:10.1002/rcm.1290070916
131. Haas MJ (1999) Fully Automated Exact Mass Measurements by High-Resolution Electrospray Ionization on a Sector Instrument. Rapid Commun Mass Spectrom 13:381–383. doi:10.1002/(SICI)1097-0231(19990315)13:5<381::AID-RCM495>3.0.CO;2-A
132. Hofstadler SA, Griffey RH, Pasa-Tolic R, Smith RD (1998) The Use of a Stable Internal Mass Standard for Accurate Mass Measurements of Oligonucleotide Fragment Ions Using Electrospray Ionization Fourier Transform Ion Cyclotron Resonance Mass Spectrometry with Infrared Multiphoton Dissociation. Rapid Commun Mass Spectrom 12:1400–1404. doi:10.1002/(SICI)1097-0231(19981015)12:19<1400::AID-RCM337>3.0.CO;2-T
133. Stenson AC, Landing WM, Marshall AG, Cooper WT (2002) Ionization and Fragmentation of Humic Substances in Electrospray Ionization Fourier Transform-Ion Cyclotron Resonance Mass Spectrometry. Anal Chem 74:4397–4409. doi:10.1021/ac020019f
134. Makarov A, Denisov E, Kholomeev A, Balschun W, Lange O, Strupat K, Horning S (2006) Performance Evaluation of a Hybrid Linear Ion Trap/Orbitrap Mass Spectrometer. Anal Chem 78:2113–2120. doi:10.1021/ac0518811
135. Scalf M, Westphall MS, Krause J, Kaufmann SL, Smith LM (1999) Controlling Charge States of Large Ions. Science 283:194–197. doi:10.1126/science.283.5399.194

136. Krusemark CJ, Frey BL, Belshaw PJ, Smith LM (2009) Modifying the Charge State Distribution of Proteins in Electrospray Ionization Mass Spectrometry by Chemical Derivatization. J Am Soc Mass Spectrom 20:1617–1625. doi:10.1016/j.jasms.2009.04.017
137. Scalf M, Westphall MS, Smith LM (2000) Charge Reduction Electrospray Mass Spectrometry. Anal Chem 72:52–60. doi:10.1021/ac990878c
138. Ebeling DD, Westphall MS, Scalf M, Smith LM (2000) Corona Discharge in Charge Reduction Electrospray Mass Spectrometry. Anal Chem 72:5158–5161. doi:10.1021/ac000559h
139. Ebeling DD, Scalf M, Westphall MS, Smith LM (2001) A Cylindrical Capacitor Ionization Source: Droplet Generation and Controlled Charge Reduction for Mass Spectrometry. Rapid Commun Mass Spectrom 15:401–405. doi:10.1002/rcm.245
140. McLuckey SA, Stephenson JL Jr (1998) Ion/Ion Chemistry of High-Mass Multiply Charged Ions. Mass Spectrom Rev 17:369–407. doi:10.1002/(SICI)1098-2787(1998)17:6<369::AID-MAS1>3.0.CO;2-J
141. Herron WJ, Goeringer DE, McLuckey SA (1996) Product Ion Charge State Determination Via Ion/Ion Proton Transfer Reactions. Anal Chem 68:257–262. doi:10.1021/ac950895b
142. Schalley CA (ed) (2007) Analytical Methods in Supramolecular Chemistry. Wiley-VCH, New York. doi:10.5301/EJO.2008.2975
143. Ramanathan R (ed) (2009) Mass Spectrometry in Drug Metabolism and Pharmacokinetics. Wiley, Hoboken. doi:10.1109/TNS.2009.2019110
144. Schalley CA, Springer A (2009) Mass Spectrometry and Gas-Phase Chemistry of Non-Covalent Complexes. Wiley, Hoboken. doi:10.3762/bjoc.5.76
145. Banoub JH, Limbach PA (eds) (2009) Mass Spectrometry of Nucleosides and Nucleic Acids. CRC Press, Boca Raton. doi:10.1109/TNS.2009.2019110
146. Williams TTJ, Perreault H (2000) Selective Detection of Nitrated Polycyclic Aromatic Hydrocarbons by Electrospray Ionization Mass Spectrometry and Constant Neutral Loss Scanning. Rapid Commun Mass Spectrom 14:1474–1481. doi:10.1002/1097-0231(20000830)14:16<1474::AID-RCM46>3.0.CO;2-Z
147. Zhu J, Cole RB (2000) Formation and Decompositions of Chloride Adduct Ions, $[M+Cl]^-$, in Negative Ion Electrospray Ionization Mass Spectrometry. J Am Soc Mass Spectrom 11:932–941. doi:10.1016/S1044-0305(00)00164-1
148. Yang C, Cole RB (2002) Stabilization of Anionic Adducts in Negative Ion Electrospray Mass Spectrometry. Anal Chem 74:985–991. doi:10.1021/ac0108818
149. Schalley CA, Ghosh P, Engeser M (2004) Mass Spectrometric Evidence for Catenanes and Rotaxanes from Negative-ESI FT-ICR Tandem-MS Experiments. Int J Mass Spectrom 232:249–258. doi:10.1016/j.ijms.2004.02.003
150. Truebenbach CS, Houalla M, Hercules DM (2000) Characterization of Isopoly Metal Oxyanions Using Electrospray Time-of-Flight Mass Spectrometry. J Mass Spectrom 35:1121–1127. doi:10.1002/1096-9888(200009)35:9<1121::AID-JMS40>3.0.CO;2-7
151. Choi BK, Hercules DM, Houalla M (2000) Characterization of Polyphosphates by Electrospray Mass Spectrometry. Anal Chem 72:5087–5091. doi:10.1021/ac000044q
152. Favaro S, Pandolfo L, Traldi P (1997) The Behavior of $[Pt(H^3\text{-Allyl})XP(C_6H_5)_3]$ Complexes in Electrospray Ionization Conditions Compared with Those Achieved by Other Ionization Methods. Rapid Commun Mass Spectrom 11:1859–1866. doi:10.1002/(SICI)1097-0231(199711)11:17<1859::AID-RCM973>3.0.CO;2-P
153. Feichtinger D, Plattner DA (1997) Direct Proof for Mn^V-Oxo-Salen Complexes. Angew Chem Int Ed 36:1718–1719. doi:10.1002/anie.199717181
154. Løver T, Bowmaker GA, Henderson W, Cooney RP (1996) Electrospray Mass Spectrometry of Some Cadmium Thiophenolate Complexes and of a Thiophenolate Capped CdS Cluster. Chem Commun:683–685. doi:10.1039/CC9960000683
155. Hinderling C, Feichtinger D, Plattner DA, Chen P (1997) A Combined Gas-Phase, Solution-Phase, and Computational Study of C-H Activation by Cationic Iridium(III) Complexes. J Am Chem Soc 119:10793–10804. doi:10.1021/ja970995u

156. Reid GE, O'Hair RAJ, Styles ML, McFadyen WD, Simpson RJ (1998) Gas Phase Ion-Molecule Reactions in a Modified Ion Trap: H/D Exchange of Non-Covalent Complexes and Coordinatively Unsaturated Platinum Complexes. Rapid Commun Mass Spectrom 12:1701–1708. doi:10.1002/(SICI)1097-0231(19981130)12:22<1701::AID-RCM392>3.0.CO;2-S
157. Volland MAO, Adlhart C, Kiener CA, Chen P, Hofmann P (2001) Catalyst Screening by Electrospray Ionization Tandem Mass Spectrometry: Hofmann Carbenes for Olefin Metathesis. Chem Eur J 7:4621–4632. doi:10.1002/1521-3765(20011105)7:21<4621::AID-CHEM4621>3.0.CO;2-C
158. Jewett BN, Ramaley L, Kwak JCT (1999) Atmospheric Pressure Ionization Mass Spectrometry Techniques for the Analysis of Alkyl Ethoxysulfate Mixtures. J Am Soc Mass Spectrom 10:529–536. doi:10.1016/S1044-0305(99)00017-3
159. Benomar SH, Clench MR, Allen DW (2001) The Analysis of Alkylphenol Ethoxysulphonate Surfactants by High-Performance Liquid Chromatography, Liquid Chromatography-Electrospray Ionisation-Mass Spectrometry and Matrix-Assisted Laser Desorption Ionisation-Mass Spectrometry. Anal Chim Acta 445:255–267. doi:10.1016/S0003-2670(01)01280-6
160. Eichhorn P, Knepper TP (2001) Electrospray Ionization Mass Spectrometric Studies on the Amphoteric Surfactant Cocamidopropylbetaine. J Mass Spectrom 36:677–684. doi:10.1002/jms.170
161. Levine LH, Garland JL, Johnson JV (2002) HPLC/ESI-Quadrupole Ion Trap Mass Spectrometry for Characterization and Direct Quantification of Amphoteric and Nonionic Surfactants in Aqueous Samples. Anal Chem 74:2064–2071. doi:10.1021/ac011154f
162. Barco M, Planas C, Palacios O, Ventura F, Rivera J, Caixach J (2003) Simultaneous Quantitative Analysis of Anionic, Cationic, and Nonionic Surfactants in Water by Electrospray Ionization Mass Spectrometry with Flow Injection Analysis. Anal Chem 75:5179–5136. doi:10.1021/ac020708r
163. Little DP, Chorush RA, Speir JP, Senko MW, Kelleher NL, McLafferty FW (1994) Rapid Sequencing of Oligonucleotides by High-Resolution Mass Spectrometry. J Am Chem Soc 116:4893–4897. doi:10.1021/ja00090a039
164. Limbach PA, Crain PF, McCloskey JA (1995) Molecular Mass Measurement of Intact Ribonucleic Acids via Electrospray Ionization Quadrupole Mass Spectrometry. J Am Soc Mass Spectrom 6:27–39. doi:10.1016/1044-0305(94)00086-F
165. Little DP, Thannhauser TW, McLafferty FW (1995) Verification of 50- to 100-Mer DNA and RNA Sequences with High-Resolution Mass Spectrometry. Proc Natl Acad Sci U S A 92:2318–2322. doi:10.1073/pnas.92.6.2318
166. Hanson L, Fucini P, Ilag LL, Nierhaus KH, Robinson CV (2003) Dissociation of Intact *Escherichia Coli* Ribosomes in a Mass Spectrometer. Evidence for Conformational Change in Ribosome Elongation Factor G Complex. J Biol Chem 278:1259–1267. doi:10.1074/jbc.M208966200
167. De Bellis G, Salani G, Battaglia C, Pietta P, Rosti E, Mauri P (2000) Electrospray Ionization Mass Spectrometry of Synthetic Oligonucleotides Using 2-Propanol and Spermidine. Rapid Commun Mass Spectrom 14:243–249. doi:10.1002/(SICI)1097-0231(20000229)14:4<243::AID-RCM870>3.0.CO;2-F
168. Greig M, Griffey RH (1995) Utility of Organic Bases for Improved Electrospray Mass Spectrometry of Oligonucleotides. Rapid Commun Mass Spectrom 9:97–102. doi:10.1002/rcm.1290090121
169. Sannes-Lowery KA, Hofstadler SA (2003) Sequence Confirmation of Modified Oligonucleotides Using IRMPD in the External Ion Reservoir of an Electrospray Ionization Fourier Transform Ion Cyclotron Mass Spectrometer. J Am Soc Mass Spectrom 14:825–833. doi:10.1016/S1044-0305(03)00335-0

170. Andersen TE, Kirpekar F, Haselmann KF (2006) RNA Fragmentation in MALDI Mass Spectrometry Studied by H/D-Exchange: Mechanisms of General Applicability to Nucleic Acids. J Am Soc Mass Spectrom 17:1353–1368. doi:10.1016/j.jasms.2006.05.018
171. McLuckey SA, Van Berkel GJ, Glish GL (1992) Tandem Mass Spectrometry of Small, Multiply Charged Oligonucleotides. J Am Soc Mass Spectrom 3:60–70. doi:10.1016/1044-0305(92)85019-G
172. Pfenninger A, Karas M, Finke B, Stahl B (2002) Structural Analysis of Underivatized Neutral Human Milk Oligosaccharides in the Negative Ion Mode by Nano-Electrospray MS^n (Part 1: Methodology). J Am Soc Mass Spectrom 13:1331–1340. doi:10.1016/S1044-0305(02)00645-1
173. Pfenninger A, Karas M, Finke B, Stahl B (2002) Structural Analysis of Underivatized Neutral Human Milk Oligosaccharides in the Negative Ion Mode by Nano-Electrospray MS^n (Part 2: Application to Isomeric Mixtures). J Am Soc Mass Spectrom 13:1341–1348. doi:10.1016/S1044-0305(02)00646-3
174. Weiskopf AS, Vouros P, Harvey DJ (1998) Electrospray Ionization-Ion Trap Mass Spectrometry for Structural Analysis of Complex *N*-Linked Glycoprotein Oligosaccharides. Anal Chem 70:4441–4447. doi:10.1021/ac980289r
175. Metelmann W, Peter-Katalinic J, Müthing J (2001) Gangliosides from Human Granulocytes: A Nano-ESI QTOF Mass Spectrometry Fucosylation Study of Low Abundance Species in Complex Mixtures. J Am Soc Mass Spectrom 12:964–973. doi:10.1016/S1044-0305(01)00276-8
176. van Duijn E, Bakkes PJ, Heeren RMA, van den Heuvel RHH, van Heerikhuizen H, van der Vies SM, Heck AJR (2005) Monitoring Macromolecular Complexes Involved in the Chaperonin-Assisted Protein Folding Cycle by Mass Spectrometry. Nat Methods 2:371–376. doi:10.1038/nmeth753
177. Breuker K, McLafferty FW (2008) Stepwise Evolution of Protein Native Structure with Electrospray into the Gas Phase, 10^{-12} to 10^{2} s. Proc Natl Acad Sci U S A 105:18145–18152. doi:10.1073/pnas.0807005105
178. Jiang W, Winkler HDF, Schalley CA (2008) Integrative Self-Sorting: Construction of a Cascade-Stoppered Hetero[3]Rotaxane. J Am Chem Soc 130:13852–13853. doi:10.1021/ja806009d
179. Jiang W, Schaefer A, Mohr PC, Schalley CA (2010) Monitoring Self-Sorting by Electrospray Ionization Mass Spectrometry: Formation Intermediates and Error-Correction During the Self-Assembly of Multiply Threaded Pseudorotaxanes. J Am Chem Soc 132:2309–2320. doi:10.1021/ja9101369
180. Jiang W, Schalley CA (2010) Tandem Mass Spectrometry for the Analysis of Self-Sorted Pseudorotaxanes: The Effects of Coulomb Interactions. J Mass Spectrom 45:788–798. doi:10.1002/jms.1769